Fabrication of Relative Humidity Sensors based on Polyimide Nanoparticles

by

YiFan Wang

B.Sc., Henan Polytechnic University, 2009

Thesis Submitted in Partial Fulfillment
of the Requirements for the Degree of
Master of Applied Sciences

in the
School of Engineering Sciences
Faculty of Applied Sciences

SIMON FRASER UNIVERSITY

Spring 2013

Approval

Name: **YiFan Wang**

Degree: **Master of Applied Sciences**

Title of Thesis: ***Fabrication of Relative Humidity Sensors based on Polyimide Nanaoparticles***

Examining Committee:

Chair: **Dr. Andrew Rawicz**, Professor

Dr. Behraad Bahreyni, P.Eng
Senior Supervisor
Assistant Professor

Dr. Ash Parameswaran, P.Eng
Supervisor
Professor

Dr. Albert Leung, P.Eng
Internal Examiner
Professor
School of Engineering Science

Date Defended/Approved: March 22, 2013

Partial Copyright Licence

Abstract

A capacitive relative humidity sensor fabricated with electrosprayed polyimide nanoparticles is proposed in this thesis. The goal has been to fabricate a humidity sensor with small size and simple structure in order to decrease the fabrication cost. Polyimide is used as the sensing material and deposited on top of the electrodes in two methods: spin-on and electrospraying. Performance of the sensors made through these two deposition methods is compared. The effect of different electrospraying parameters on the sensor performance are studied and discussed. The sensor output was measured and compared using a capacitance sensing circuit, an oscillator circuit, and a standard LCR meter. Experimental results show that the humidity sensors proposed in this thesis provide stable data in a short time with low hysteresis when increasing and decreasing humidity. The technique is flexible and can be used to build relative humidity sensors directly on printed circuit board, thus reducing manufacturing costs of such sensor systems.

Keywords: Relative humidity sensor; Electrospraying; Polyimide; Nanoparticles; Spin-on films; Capacitive interface

To my parents and all the other people I love

Acknowledgements

I would like to thank, first and foremost, my senior supervisor Dr. Behraad Bahreyni. I am grateful to pursue my master study under his supervision. He is a great teacher who not only teaches me how to conduct researches but more important let me know the attitudes of being a successful researcher and engineer. During these years of study, I had a lot of challenges; fortunately he is a great coach to encourage me and try his best to help me to overcome those difficulties. Without his patient and valuable help, this thesis would have remained a dream. I would like to thank him from the deep of my heart.

It gives me great pleasure in acknowledging the support and help of my supervisor Dr. Ash Parameswaran. We had a lot of wonderful discussions, which helps me to formulate my ideas on how to test relative humidity sensor. I really appreciate it that he let me use his polyimide PI-2611 in my project.

I am deeply grateful to Dr. Albert Leung for being on my committee and reviewing my thesis and gave me lots of valuable advices about my thesis.

I am sincerely thankful to Dr. Andrew Rawicz for being the chair of my committee and reading my thesis. Thanks to Dr. Woo Soo Kim for providing LCR meter which is necessary for precise capacitance measurement.

I would like to thank all my labmates in IMuTS lab especially Sadegh, Amin, and Mona.

Last but not least, I would like to take this opportunity to thank my parents, Lanli Wang and Fenglian Ren, for their constant support and selfless love.

Table of Contents

List of Tables

List of Figures

List of Acronyms

C-F	Capacitance to Frequency Converter
C-V	Capacitance to Voltage Converter
DI Water	Deionized Water
D PT	Dew Point
FM	Flow Meter
F PT	Frost Point
IDE	Interdigitated Electrode
MEMS	Microelectromechanical systems
PCB	Printed Circuit Board
PI	Polyimide
PR	Photoresist
QCM	Quartz Crystal Microbalance
RH	Relative Humidity
RIE	Reactive Ion Etching
SAW	Surface Acoustic Wave
SEM	Scanning Electron Microscope

1. Introduction

1.1. Motivation and Background

Humidity measurement and control are important in numerous medical, industrial, and agricultural applications. In medical field, humidity control is required during pharmaceutical processing. In industry, many manufacturing processes such as semiconductor manufacturing and chemical gas purification rely on well-controlled levels of humidity. In agriculture, greenhouse and incubation need humidity control. Humidity control is also important in humans' daily lives. The ideal indoor relative humidity (RH) should be between 35% and 65%. Lower RH levels cause discomfort and health problems such as chapped lips, bleeding nose, and dry throat [1]. Higher RH levels, on the other hands, cause fungus growth. All of these applications plus many more make humidity control more important nowadays.

In 1450, Nicolas Cryfts invented a hygrometer which is the first humidity measurement instrument on record. This hygrometer used wool to determine the changes of humidity in air [2]. After hundreds of years of development, many kinds of hygrometer were invented, such as psychrometer and Lithium chloride (LiCl) dew point sensor. These methods are referred to as classical humidity measurement techniques. Compared to modern instruments, these devices have large size, slow response, and often have low accuracy. The development of miniaturized humidity sensors is growing in par with the demand for them [3]. Miniaturized humidity sensors have many advantages compared to the classical measurement mentioned in the previous parts including: integration, small size, low power consumption, high performance, low cost, and ease of mass fabrication [4].

Making a good humidity sensor is based on many considerations, such as accuracy, power consumption, precision, repeatability, long-term stability, response time, size, packaging, and cost [5]. Nowadays, size and cost become more and more important among all these specifications.

There are many humidity sensors in the market. Throughout this thesis, we rely on two standard RH sensors as benchmark, for result comparison. These two devices are HM 1500 and HIH-4000-003 whose responses are shown in Figure 1.1 and 1.2.

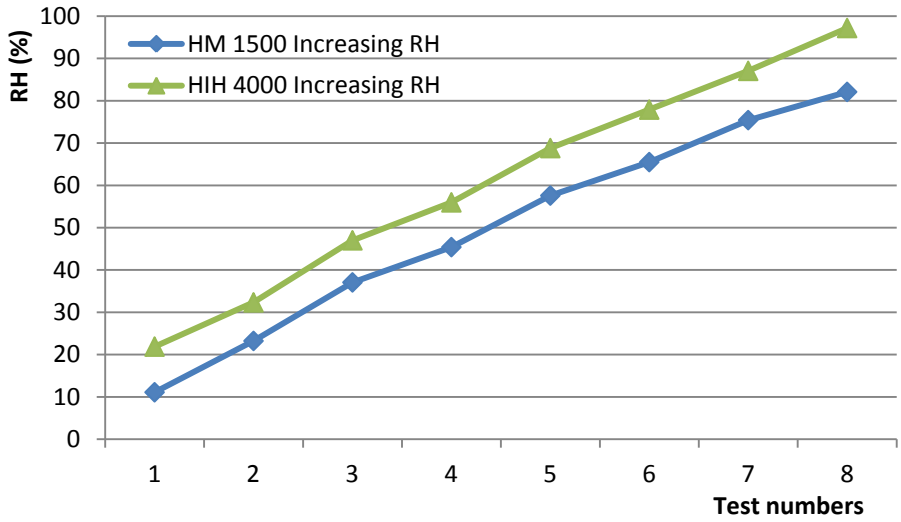

Figure 1.1: Comparison of the RH readings from two commercial humidity sensors tested side-by-side (HM 1500 and HIH-4000-003). There is a near 10% difference in RH readings from these sensors over their operating range.

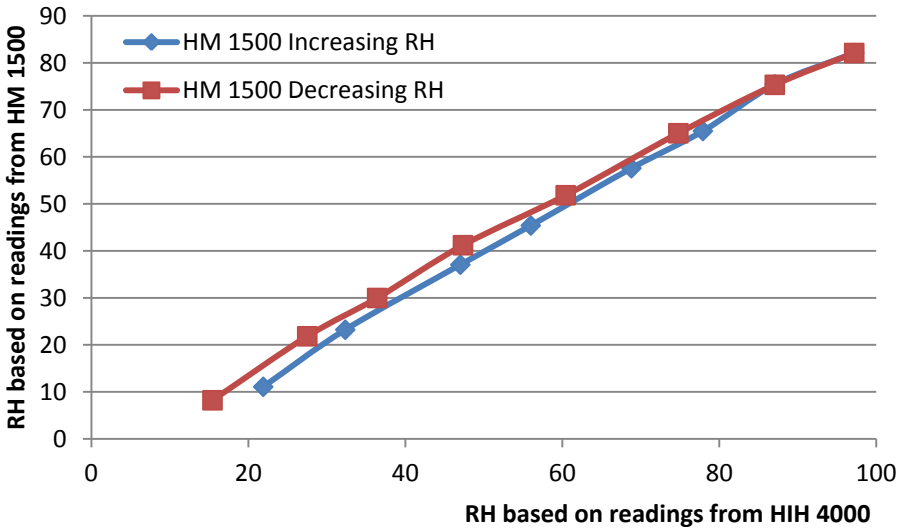

Figure 1.2: Repeatability between increasing RH and decreasing RH of commercial humidity sensors HM 1500 using HIH-4000-003 as the reference.

"Increasing RH" in the Figures 1.1 and 1.2 means the data was taken when the RH was increased and the "Decreasing RH" in Figure 1.2 means the data is taken when the RH was reduced. The RH detected by HIH-4000-003, "HIH 4000 Increasing RH", is used as the reference. Both sensors were put inside a humidity chamber and data from both sensors was read at the same time.

The reported accuracy and hysteresis of humidity sensor HIH-4000-003 are ±3.5%RH and 3%RH, respectively. HM 1500's accuracy and hysteresis are ±5%RH and ±1.5%RH, respectively. As shown in Figure 1.1, the RH detected by HIH-4000-003 is around 10% higher than the RH detected by HM 1500, even though both sensors are made similarly. It is hard to tell which sensor detects the current RH. We use HIH-4000-003 as the primary reference due to its better packaging. Figure 1.2 shows the repeatability of the output voltage between increasing and decreasing RH of HM 1500 based on humidity sensor HIH-4000-003. As shown in Figure 1.2, humidity sensor HM 1500 has poor repeatability from 20% to 80% RH. The price of the humidity sensor HM 1500 is about $45, and HIH-4000-003 is about $25. Despite their high cost, it is hard to know the exact RH using either of these humidity sensors. The purpose of this thesis is to fabricate a working RH sensor with low cost.

1.2. Outline of the thesis

This thesis discusses a relative humidity sensor with electrosprayed polyimide nanoparticles to reduce the number of fabrication steps compared to sensors made with a uniform film of polyimide that is deposited through a spin-on process.

In Chapter 2, literature review about humidity sensor is presented. The classification and units for humidity are presented first. Then the classical humidity measurement techniques including psychrometer, hair hygrometer, LiCl dew point sensor, and chilled mirror hygrometers are introduced. Miniaturized humidity sensors, which can be categorized into capacitive, resistive, thermal conductivity, optical, and gravimetric sensors, are discussed at the end of humidity sensor part.

The principle and application of electrospraying and electrospinning are discussed in Chapter 3. The background about electrospraying/electrospinning is

mentioned first and followed by the discussion on Taylor cone and electrospraying controlling parameters.

Sensor fabrication steps are explained in Chapter 4. Electrode design and patterning are introduced first. Then spin-on and electrosprayed nanoparticle polyimide deposition methods are discussed and compared.

Chapter 5 discusses the interface electronics used for measuring capacitance of the sensor. Two kinds of circuits, capacitive sensing circuit and oscillator circuit, are discussed in this chapter.

Experimental results are discussed in Chapter 6. The measurements with three different methods including capacitive sensing circuit, oscillator circuit, and LCR meter are explained first. Advantages and disadvantages of these three methods are discussed. Data from devices with uniform thin films and electrosprayed nanoparticles are presented afterwards. The effects of electrospraying parameters are also discussed in this chapter.

In Chapter 7, conclusions, contributions, and future work are mentioned.

2. Humidity Sensing

Humidity is the amount of water vapor in air. A humidity sensor detects the concentration of water vapor in a pure gas or a mixture of gases, such as air. Humidity can be expressed in many ways including *absolute humidity* and *relative humidity* [6]. Absolute humidity is the mass of the water vapor in a given volume, whose unit is mg/ml or g/m^3. It is however difficult to measure the mass of the water vapor makes relative humidity a more common used measurement.

Relative humidity and Dew/Frost point (D/F PT) are the two commonly used units for reporting humidity levels [7]. RH is the ratio of partial vapor pressure in a unit volume to the saturation vapor pressure in the unit volume at a particular temperature and is usually specified as a percentage. RH is a strong function of temperature; it will change when temperature changes even if the absolute humidity has not changed. Dew point is the temperature at which the water vapor in the air will condense into liquid water; i.e., Dew point equals the air temperature when RH is 100%. Frost point is the temperature at which the water vapor in the air condenses to ice without passing liquid phase. As a result, frost point is always below 0°C. Dew and frost point are absolute measurements. However, relative humidity is the most commonly used unit for reporting humidity levels for two reasons: (1) the temperature range for most applications that require humidity control is fairly narrow; and (2) RH sensors are considerably less expensive than other types of humidity sensors.

2.1. Classical Humidity Measurements

There are several methods for measuring humidity. Psychrometer, hair hygrometer, LiCl dew point sensor, and chilled mirror hygrometers are just a few of the more common methods. All of these methods have their own advantages and disadvantages, which are briefly discussed below.

2.1.1. Psychrometer

The psychrometer consists of two bulb thermometers (see Figure 2.1). One thermometer is covered by cotton wick which contains water or ice. This thermometer is called “wet bulb” and measures the temperature of adiabatic saturation. The other thermometer is uncovered to measure room temperature. This thermometer is called “dry bulb”. The wet bulb needs to consume heat to evaporate water, so the temperature in wet bulb is always lower than it in dry bulb.

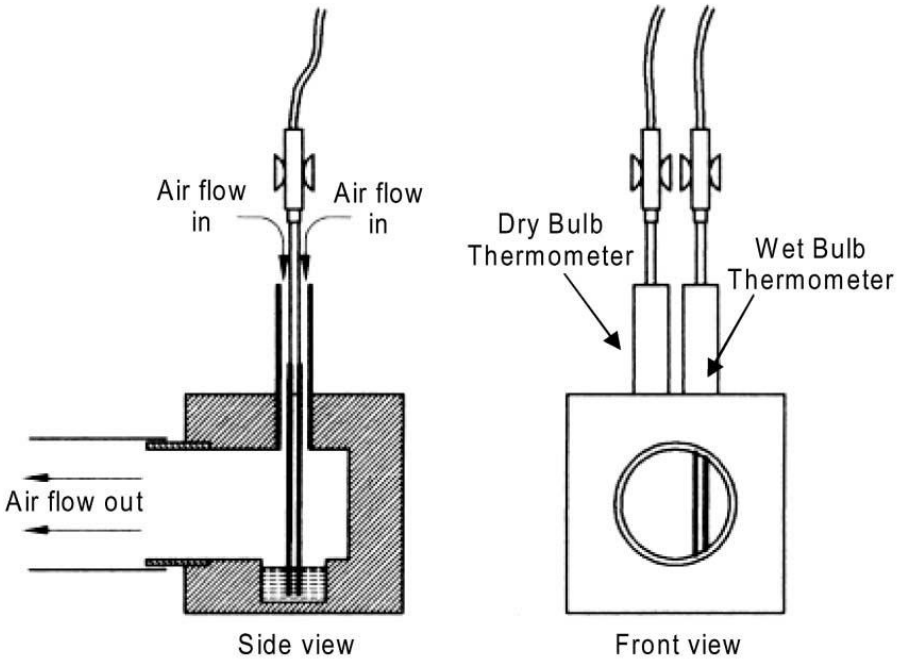

Figure 2.1: The schematic of psychrometer [8].

The temperature difference between wet bulb and dry bulb is related to the ambient humidity. When the humidity is lower, the water is evaporated more easily in wet bulb. The temperature therefore drops more in wet bulb. However, the temperature difference is also related to many other factors, such as air flow, air pressure, and the diameter of the bulb. The advantage of psychrometer is its accuracy, which relies on the physical properties of water. The disadvantages include its size, power consumption, and the need for regular maintenance, such as replenishing of water [8].

2.1.2. Hair Hygrometer

Many natural materials are sensitive to humidity, such as hair, wood, and paper. Dimensions of these materials change with humidity. Hair hygrometer (see Figure 2.2) was invented by De Saussure in 1783 based on this principle [9].

The amount of moisture hair can absorb is depended on the amount of relative humidity in the ambient. On the other hand, the length of the hair is related to the moisture it contains. The length of the hair will increase when the relative humidity is increasing. A piece of hair is easy to broken, so a brunch of hair is usually used to increase the mechanical strength. The position of the pointer will change as the length of the hair changes. The hair hygrometers are cheap, simple, and easy to be used. The disadvantages are low accuracy and slow response as well as size.

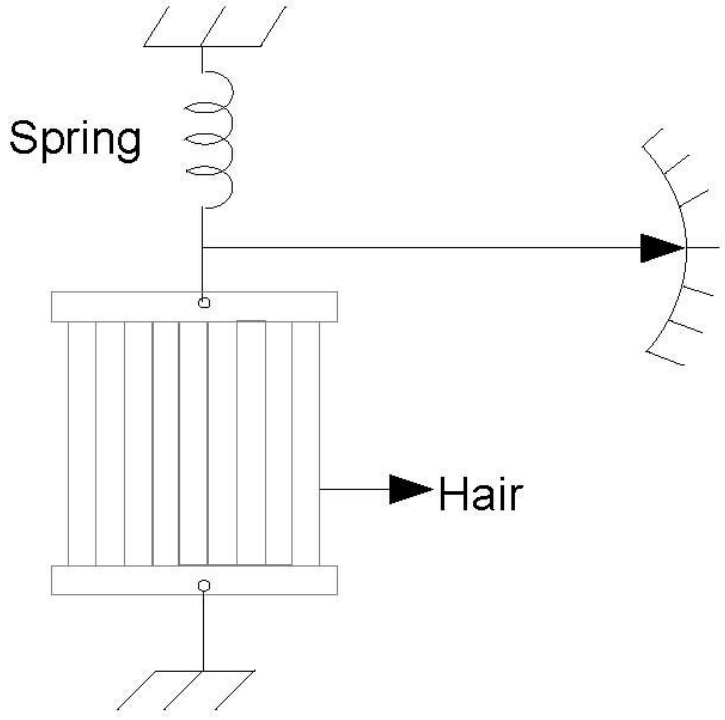

Figure 2.2: Hair hygrometer schematic [9].

2.1.3. Lithium Chloride Dew Point Sensor

LiCl shows good stability in air. LiCl is in solid state and has high resistance when humidity is below than 12% RH. When RH increases to 12%, LiCl will absorb moisture in the air and deliquescence into a liquid state. Therefore, the LiCl dew point sensor can only work when RH is more than 12%.

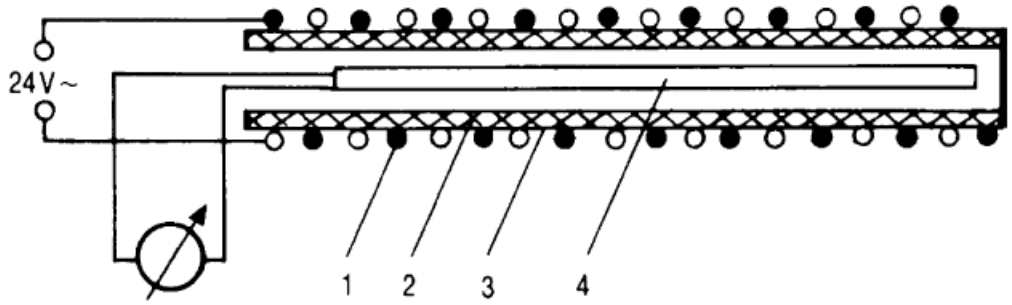

Figure 2.3: LiCl dew point sensor schematic: (1) heating electrode; (2) wick soaked with LiCl; (3) metal housing and (4) measurement electrode [8].

Dilute LiCl solution is coated on a thin walled glass tube which has two thin copper wires wound around it [8]. The schematic of the LiCl dew point sensor is shown in Figure 2.3. When RH is above 12%, LiCl will deliquescence into solution. As RH increase, LiCl absorbs more moisture, and there are more conductive ions in LiCl therefore reducing resistance. When a fixed voltage is applied to the wires, there will be higher current with lower resistance, so the sensor is heated. The water in LiCl will evaporate because of heating which leads to higher resistance. This process will stop and the temperature will be stable when equilibrium between LiCl solution and RH is reached. The temperature then read and related to RH or dew point. The main advantage of the LiCl dew point sensors are their accuracy. However, they have a long response time and require regular maintenance.

2.1.4. Chilled Mirror Hygrometers

In these sensors, the gas sample flows over the mirror under a given pressure, when the temperature is lowed to a point that makes dew appear at the surface of the mirror, the temperature of the mirror is the dew point. The mirror used in the chilled

mirror hygrometers is usually made of a material with good thermal conductivity such as silver or copper. Some inert metal was to be used for preventing tarnishing and oxidation such as iridium, rubidium, nickel, or gold [10]. A thermoelectric cooler is used to chill the mirror. The mirror surface is illuminated by a beam of light and the reflected light is monitored by a photodetector (see Figure 2.4). The reflected light disperses when the dew droplets form on the mirror surface. The photodetector output will decrease with the decreasing reflected light. The thermoelectric heat pump is in turn controlled via a control system. A precision miniature platinum resistance thermometer is embedded in the mirror to maintain the mirror temperature at the dew point.

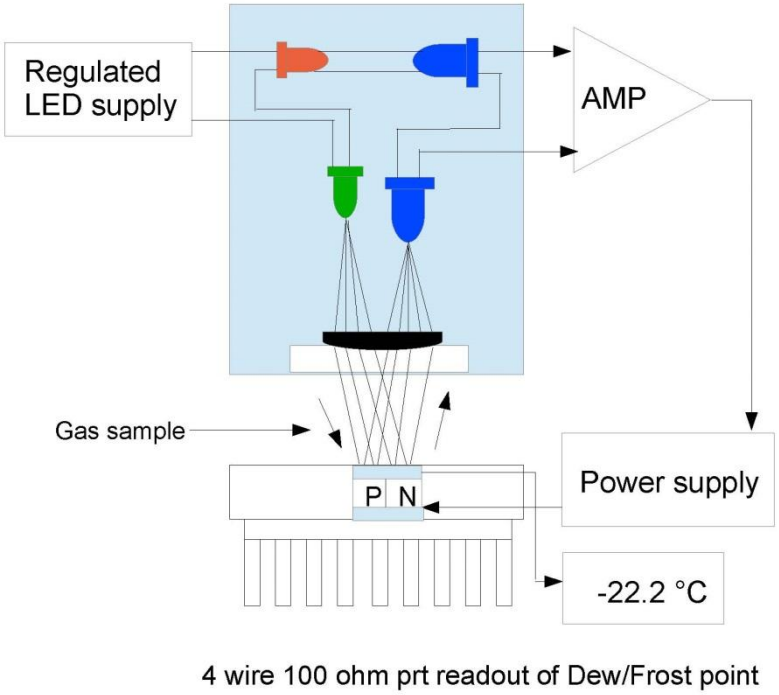

Figure 2.4: Block diagram of chilled mirror hygrometer [10].

The sensor is measuring the dew point when the mirror temperature is above the ice point. Below 0°C, the sensor is measuring the frost point. Absolute humidity can be calculated from dew/frost point, and relative humidity can be extracted from dew/frost point and gas temperature. The advantages of chilled mirror hygrometer are its high

accuracy and long-term stability. The disadvantage is that the mirror should be kept clean which requires care and attention during the experiment and frequent maintenance. Nonetheless, chilled mirror hygrometers are often used as the reference sensors in applications where accuracy is needed.

2.2. Miniaturized Humidity Sensors

Miniaturized humidity sensors are becoming popular for they have many advantages compared to afore mentioned classical measurement. Microelectromechanical systems (MEMS) are among the methods for making miniaturized sensors. According to the sensing principles, miniaturized humidity sensor can be divided into five categories: resistive, thermal conductivity, optical, gravimetric, and capacitive [11].

2.2.1. Resistive Humidity Sensors

The resistance of a given object is dependent on two factors: the material and its shape. The resistance of a material with a constant crosssection, R, can be calculated from:

$$R = \rho \frac{L}{A} \tag{4}$$

where ρ is the electrical resistivity, L is the length of the conductor, and A is the cross-section area of the conductor. When the resistor is exposed to humidity, the ionic functional groups will be dissociated to increase the electrical conductivity of the resistor, which results in the decreasing of resistance.

A resistive humidity sensor with 3-Aminopropyltriethoxysilane (APTS) and n-butyl bromide (BB) is shown in [12]. APTS and BB are mixed together in ethanol, and are then deposited on a ceramic substrate which has interdigitated gold electrode on top. This resistive humidity sensor exhibits good sensitivity over a wide RH range (11% to 97%) and small hysteresis (about 1% RH). The sensor also has good environmental stability and high water-resistance which are proved by experiment.

A resistive humidity sensor using zinc oxide nanowires (ZnO NWs) as the sensing material was presented in [13]. Si wafers with thermally grown oxide were used as the substrate. ZnO NWs is placed between freestanding gold electrodes which are fabricated on top of the substrate. Due to the high surface-volume-ratio and large exposed NW surface, the resistive humidity sensor can absorb water molecules easily.

Plasma-treated multiwall carbon nanotube/polyimide (p-MWCNT/PI) is used as the sensing material in [14]. A Si_3N_4 bridge was fabricated on top of the Si substrate. Pt/Ta electrodes were then deposited on the top of Si_3N_4. The MWCNT/PI film is deposited on top of Si_3N_4 between the electrodes. The resistive humidity sensor with MWCNT/PI film exhibited better linearity over a wide RH range and lower resistance compared to the sensor only composed of polyimide. Most resistive humidity sensors show highly nonlinear response.

2.2.2. Thermal Conductivity Humidity Sensors

Thermal conductivity is the property of a material's ability to conduct heat in physics. A thermal conductivity humidity sensor, which measures the difference of thermal conductivity between dry air and air containing water vapor, is an absolute humidity sensor. The temperature of an object can be changed more easily in dry air than when air contains water vapor [15].

Thermal conductivity humidity sensors consist of two matched thermistors [15]. These two thermistors are put in the same DC bridge circuit. One of the thermistors is reference which is sealed in dry nitrogen, while the other one is for testing the absolute humidity which is exposed to ambient (see Figure 2.5). The output voltage of the DC bridge circuit is proportional to absolute humidity.

A thermal conductivity humidity sensor fabricated in a standard CMOS process was presents in [16]. Two suspended p-n junction diodes, which are used to isolate from the substrate, are used in this sensor. One of the diodes is sealed by attaching a silicon cap as the reference diode. The other diode is the test diode which is exposed in the environment. The results showed that this sensor has good sensitivity, low power consumption, and low cost.

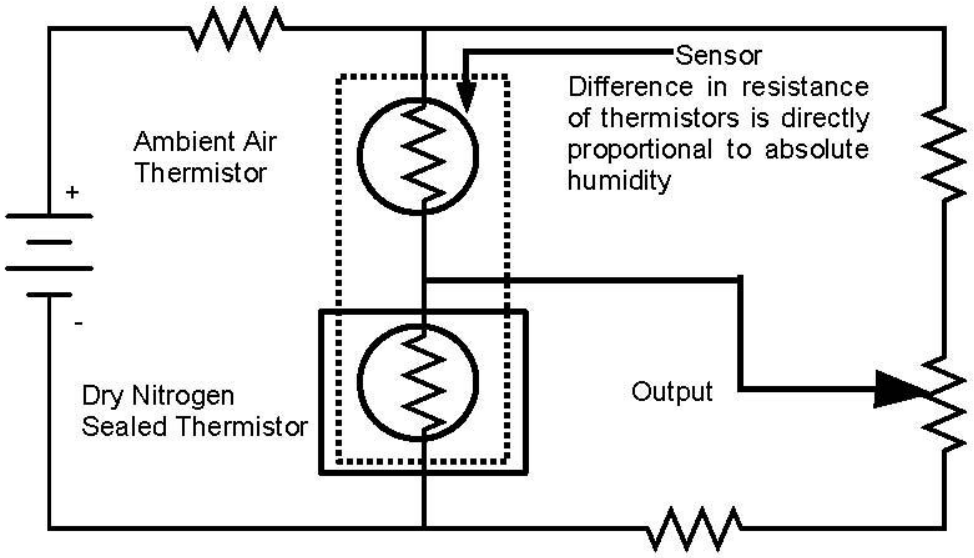

Figure 2.5: Thermal conductivity humidity sensor [15].

2.2.3. Optical Humidity Sensors

Optical humidity measurement can be based on the amplitude, the polarization, and the frequency change as a function of humidity [8]. When the sensor is coated with humidity-sensitive film, the refractive index of the film will change when absorbing water vapor. The humidity can be detected depends on the change of refractive index [17].

One example of using humidity-sensitive polymers for optical RH sensor was presented in [18]. The sensitivity of the sensor is improved with humidity-sensitive polymer infiltrating the micro-holes of a photonic crystal fiber (PCF) compared to the sensor without polymer. This sensor has the advantages of compact length, low cost and simple fabrication.

Cobalt chloride ($CoCl_2$) doped PVA/SiO_2 film is another humidity-sensitive film coated on optical humidity sensor [19]. This sensor could detect the humidity form 25% to 65% according to the change of water absorption of $CoCl_2$ - PVA/SiO_2 film. The sensing material PVA/SiO_2 was a stable material which gives this sensor a good stability.

Aitor Urrutia presented an optical humidity sensor with poly(acrylic acid) (PAA) electrospun nanofibers as the sensing film [20]. Electrospinning was employed to deposit the PAA film onto the humidity sensor.

2.2.4. Gravimetric humidity sensors

The gravimetric measurement is based on the mass change that is caused by the hygroscopic material's humidity absorption. Humidity can be detected by the change of resonant frequency which is caused from the change of mass [21].

Pascal-Delannoy described a gravimetric humidity sensor based on Quartz Crystal Microbalance (QCM) and a Peltier module [21]. The Peltier element is attached directly with the crystal. The contact between the Peltier element and the quartz was made using silver grease to improve thermal conductivity. By comparing the quartz sensor frequency to quartz reference frequency, we can know the delay time to detect the RH. The result showed that this sensor could measure the RH range from 20% to 95% with a fast response time and good accuracy.

Another example of gravimetric humidity sensor is a surface acoustic wave (SAW) humidity sensor using electrosprayed polymerized electrolyte nanoparticles as the humidity sensing film [22]. This sensor had a wide RH detection range, high sensitivity, repeatability, and fast response time.

A novel gravimetric humidity sensor, which is based on flexural resonant frequency changes of alumina cantilever beams subject to piezoelectric excitation, is presented in [23]. This sensor are coated with poly(N-vinylpyrrolidinone) (PNVP) and poly(ethyleneglycol) (PEG) to detect RH. This sensor shows a good sensitivity in a wide RH range (12% ~ 85%).

2.2.5. Capacitive Humidity Sensors

The capacitance of two parallel plates, C, can be calculated as follows:

$$C = \varepsilon_r \varepsilon_o \frac{A}{d} \tag{1}$$

where A is the overlap area of the two parallel plates, ε_r and ε_o are dielectric constant and electric permittivity ($\varepsilon_o \approx 8.854 \times 10^{-12} Fm^{-1}$), respectively, and d is the distance between the two parallel plates.

Capacitive RH sensors are widely used because of their linearity in a wide range of RH [24]. Operation of capacitive RH sensors is based on the change of the dielectric constant of a sensitive material as a function of the RH in the surrounding environment [25]. Several different materials are used as sensing elements for humidity sensor; ceramics, and polymers are the two mostly used types [7] [26].

In presence of water vapor, the dielectric constant, ε_r, of air can be calculated from [27]:

$$\varepsilon_r = 1 + \frac{211 \times 10^{-6}}{T}\left(P + \frac{48 P_s}{T} RH\right) \quad (2)$$

where T is the absolute temperature, P and P_s are the pressure of moist air and saturated water-vapor at temperature T, and RH is the relative humidity.

Equation (1) shows that capacitance C is proportional to dielectric constant ε_r; equation (2) shows that dielectric constant ε_r is proportional to relative humidity, RH. So the capacitance C is approximately proportional to relative humidity RH which is shown as follows [27]:

$$C_h \approx C_o(1 + \alpha_h RH) \quad (3)$$

where C_o is the capacitance C when RH is 0%.

TiO_2, which is one of the basic types of oxide-based ceramic [7], is used for making capacitance humidity sensors [28]. A capacitive humidity sensor was fabricated using nanostructured TiO_2, which was produced by glancing angle deposition (GLAD), as the sensing material. A coplanar interdigitated electrode (IDE) structure was used for this sensor (see Figure 2.6). The advantage of this sensor is its wide range sensitivity and fast response time.

Due to its stability at elevated temperatures and at wide range of RH, Al_2O_3 is one of the most used ceramic sensing materials. Using aluminum as the substrate, micro-sized anodic aluminum oxide (AAO) sensors where fabricated on silicon chips as

discussed in [25]. The top view and cross section of this capacitive humidity sensor is shown in Figure 2.7. This AAO based humidity sensor has a high sensitivity which is around 15pF/RH% on average.

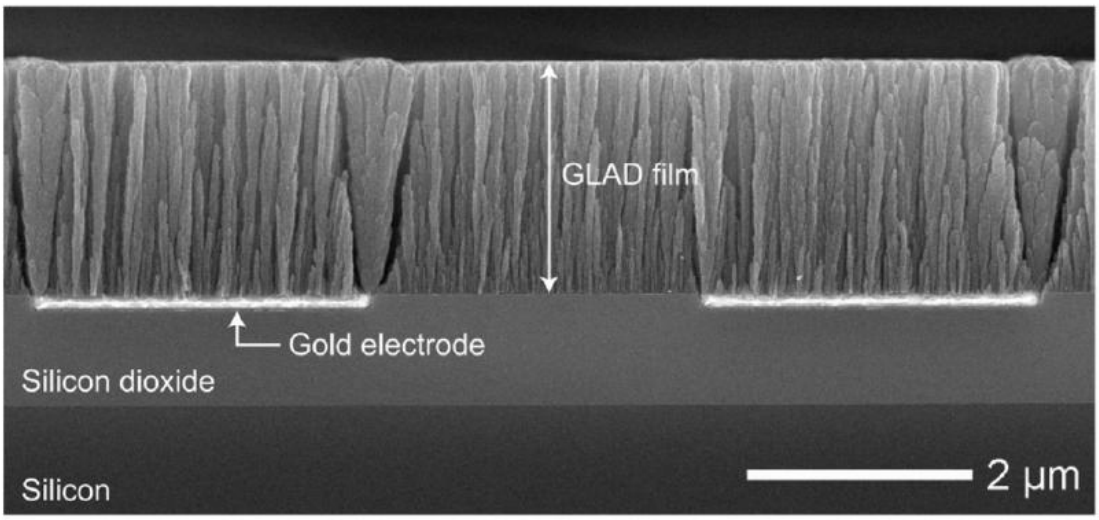

Figure 2.6: Cross-scetion of the TiO_2 based humidity sensor under SEM [28] © [2007] IEEE. Reprinted, with permission, from [J. Steele, G. Fitzpatrick and M. Brett, Capacitive humidity sensors with high sensitivity and subsecond response times, IEEE Sensors Journal, June 2007].

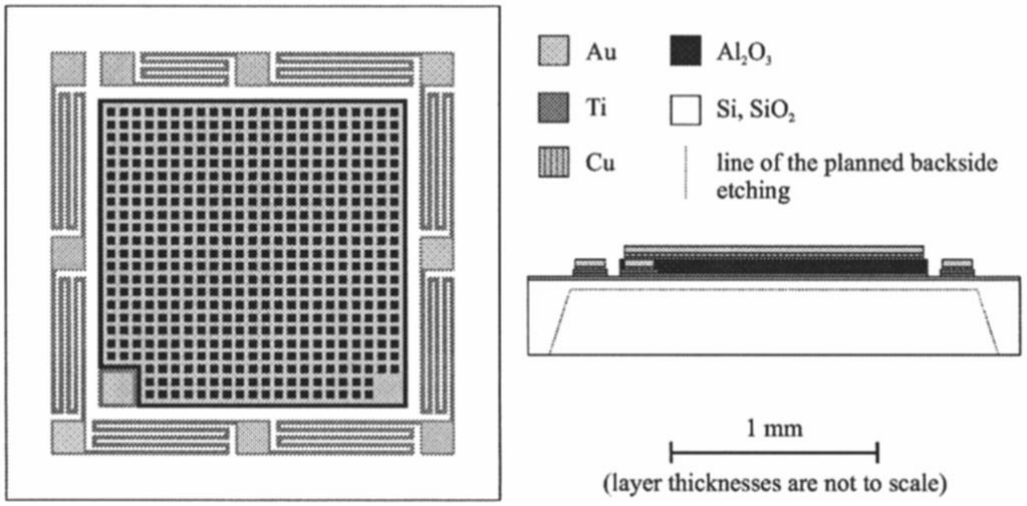

Figure 2.7: Top view (left) and cross-section (right) of the porous alumina based RH sensor [25] © [2008] IEEE. Reprinted, with permission, from [J L. Juhasz, A. Vass-Vamai, V. Timar-Horvath, M. Desmulliez and R. Dhariwal, Porous alumina based capacitive MEMS RH sensor, Symposium on Design, Test, Integration and Packaging of MEMS/MOEMS, 2008].

A novel capacitive humidity sensor which uses porous silicon as the sensing material is presented in [29]. This sensor includes a capacitor with a porous silicon dielectric, a refresh resistor, and two thermoresistors. The sensitivity of the capacitor and the reproducibility of the sensor properties are largely dependent on how the porous silicon is electrically contacted. Figure 2.8 shows three examples of the electrode configuration. This humidity sensor has good stability on mechanical and thermal parts.

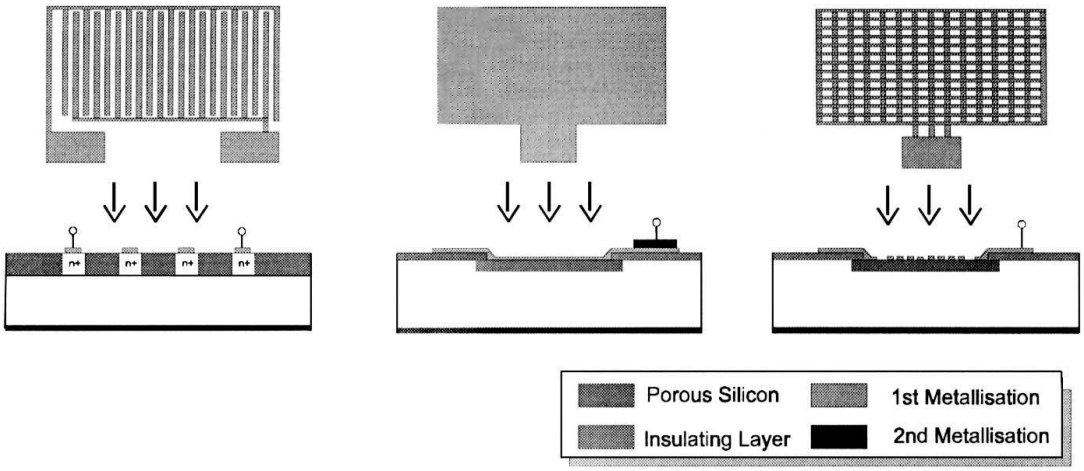

Figure 2.8: Three examples of the electrode configurations: interdigital electrodes (left), plate electrode (middle), and meshed plate electrode (right). [29].

Huebnerite ($MnWO_4$) is another sensing material for ceramic humidity sensors [30]. The humidity sensor is fabricated with a sandwich structure by depositing the $MnWO_4$ between two interdigitated electrodes (see Figure 2.9). Alumina is used as the substrate and heaters are fabricated on the backside of the substrate. LiCl powders, instead of traditional glass frits, are used as adhesion promoters in this paper. High sensitivity and fast response are the advantages of this humidity sensor.

An example of the polymer based humidity sensor is a fast response capacitive humidity sensor made using divinyl siloxane benzocyclobutene (DVS-BCB) [31] [32]. The sensor is fabricated with parallel electrodes and coated with DVS-BCB which is shown in Figure 2.10. As it shown in the experimental result, if the width of the upper

electrodes and the spacing between the upper electrodes are the same, the sensor with smaller width and spacing has a higher sensitivity and faster response.

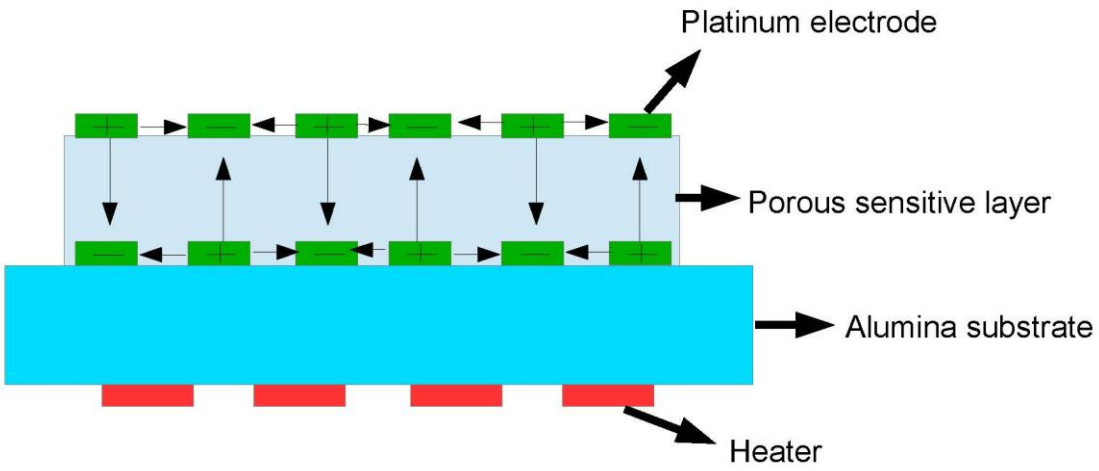

Figure 2.9: Cross-section of the $MnWO_4$ based ceramic humidity sensor with sandwich structure [30].

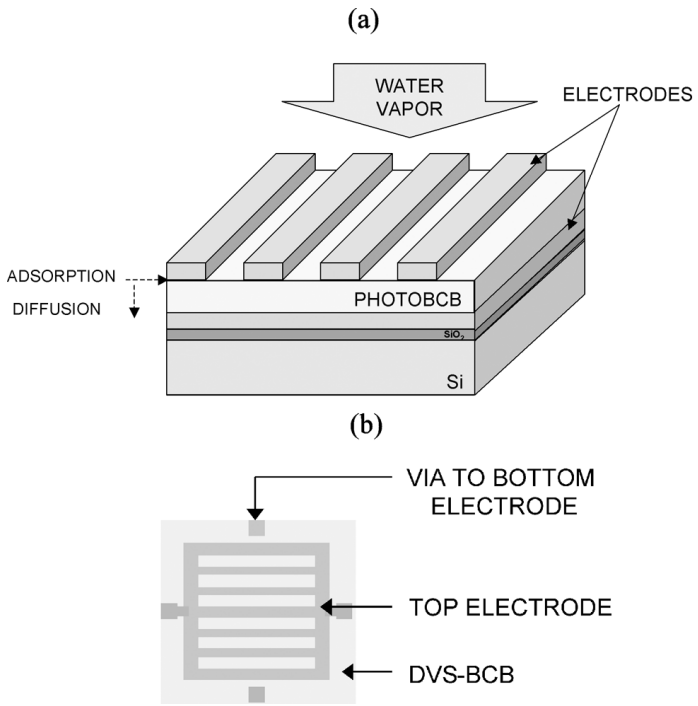

Figure 2.10: Cross-section (a) and top view (b) of the DVS-BCB based humidity sensor [31] © [2006] IEEE. Reprinted, with permission, from [A. Tetelin and C. Pellet, Modeling and optimization of a fast response capacitive humidity sensor, IEEE Sensors Journal, June 2006].

Polyimide (PI) has been used as the sensing material due to its low hysteresis, linear behavior, and stability over a wide temperature range [4]. A capacitive humidity sensor with a novel PI design is discussed in [4]. The humidity sensor has a cavity on a silicon substrate to improve reliability. Al bottom electrode, a PI sensing layer, and a comb-shaped Al top electrode with branches make up the sensor (see Figure 2.11). The capacitive humidity sensor with etched PI layer had 350 fF/%RH sensitivity and 40 seconds response time compared to 303 fF/%RH sensitivity and 122 seconds response time of the sensor with non-etched PI layer. The high sensitivity and low response time are the advantages of this capacitive humidity sensor.

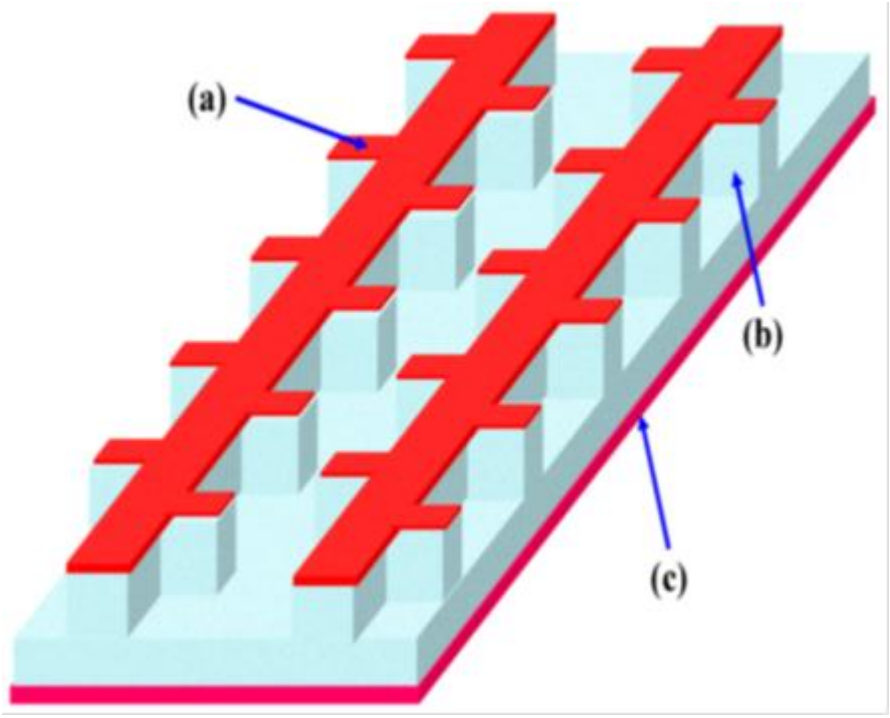

Figure 2.11: Top view of the PI based capacitive humidity sensor: (a) top electrode with branches, (b) PI layer, and (c) bottom electrode [4] © [2009] IEEE. Reprinted, with permission, from [J.-H. Kim, S.-M. Hong, J.-S. Lee, B.-M. Moon and K. Kim, High sensitivity capacitive humidity sensor with a novel polyimide design fabricated by MEMS technology, 4th IEEE International Conference on Nano/Micro Engineered and Molecular Systems, Jan 2009].

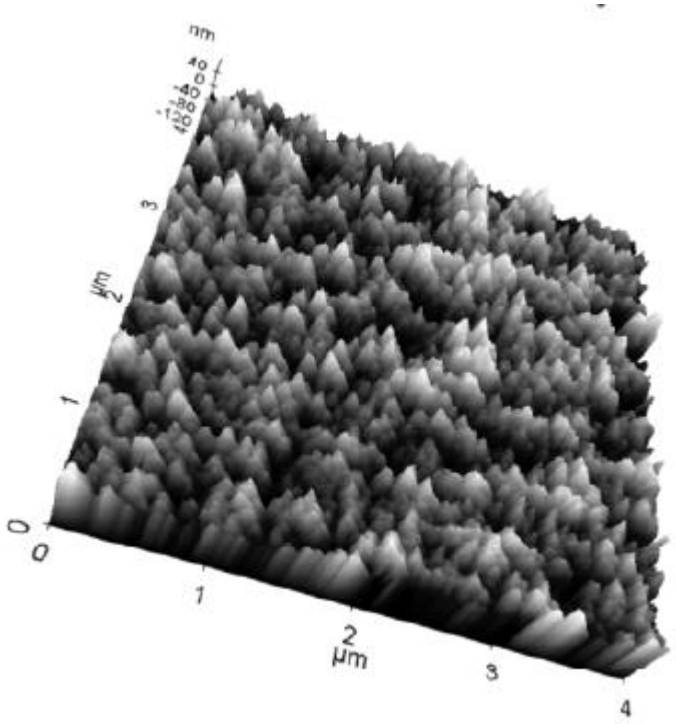

Figure 2.12: AFM image of nano-grass polyimide [33] © [2009] IEEE. Reprinted, with permission, from [H. Lee, S. Jung, H. Kim and J. Lee, High-performance humidity sensor with polyimide nano-grass, International Solid-State Sensors, Actuators and Microsystems Conference, TRANSDUCERS 2009, June 2009].

Hyemin Lee also fabricates a humidity sensor using polyimide as the sensing material [33]. The nano-grass PI is on top of the interdigitated gold electrodes as the moisture sensing material. The AFM image of the nano-grass PI is shown in Figure 2.12. This humidity sensor offers efficient adsorption of water for its nano-grass surface area is 21 times of the flat surface. The nano-grass structure makes the humidity sensor have a higher sensitivity and faster response time.

3. Electrospraying and electrospinning

Electrospraying and electrospinning processes have attracted significant attention due to their outstanding characteristics. Nano-sized particles and fibers with diameters ranging in the nanometer range can be simply fabricated through electrospraying and electrospinning, respectively. Nano-structure provides several advantages such as high surface to volume ratio, nano-porosity, and enhanced mechanical properties. Electrospraying and electrospinning therefore have many applications, such as electrospray ionization, air purification, liquid metal ion sourcing, protective clothes, sensors, and conducting devices.

William Gilbert in the late 16th century discovered the electrospraying process. He used electrically charged amber to electrospray a droplet of water [34]. The first documented records of electrospinning are patents by J.F. Colley in 1900 and W.J. Morton in 1902 [35].

A simple setup can be used for both electrospraying and electrospinning as shown in Figure 3.1. The electrospraying setup includes a high voltage power source, a syringe pump, a syringe with metal needle, and a collector [36]. The syringe pump very slowly pushes the fluid through the metal needle. For the liquid at the tip of the needle, there will be two opposite forces when the high voltage power source is turned on. One force is the surface tension of the liquid and the other is the electrostatic repulsive force due to the charge build up in the fluid. When these two forces are balanced with each other, the liquid takes the shape of a cone (see Figure 3.2), which is known as Taylor cone for the contribution of Sir Geoffrey Taylor in 1964. Taylor further discussed the fundamental principle of the formation of droplets placed in an electric field [35]. As the voltage is increased, the electrostatic repulsive force will increase. When the electrostatic repulsive force becomes larger than the surface tension, the liquid will jet from the tip of the Taylor cone towards the grounded collector [37]. For electrospraying and electrospinning, the Taylor cone looks the same, but the jets are different (see Figure 3.2).

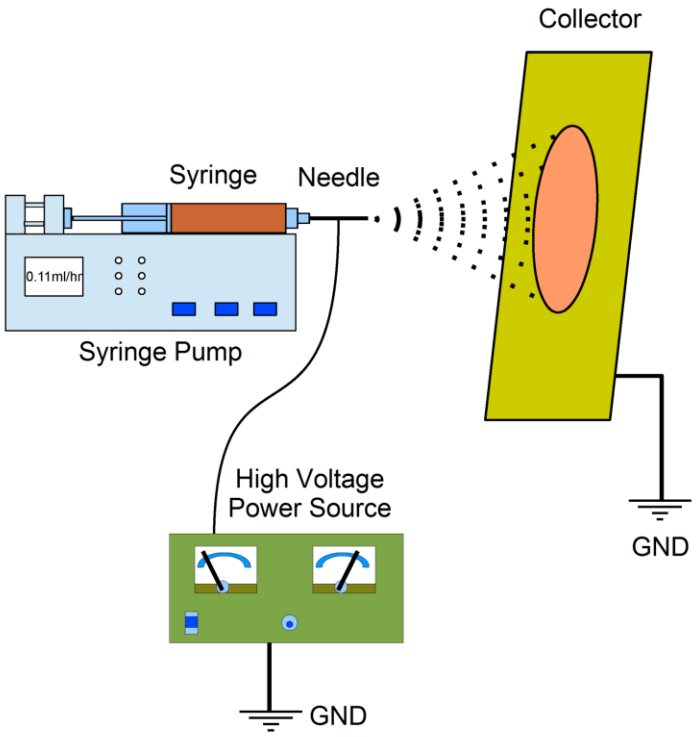

Figure 3.1: Schematic of electrospraying and electrospinning set-up.

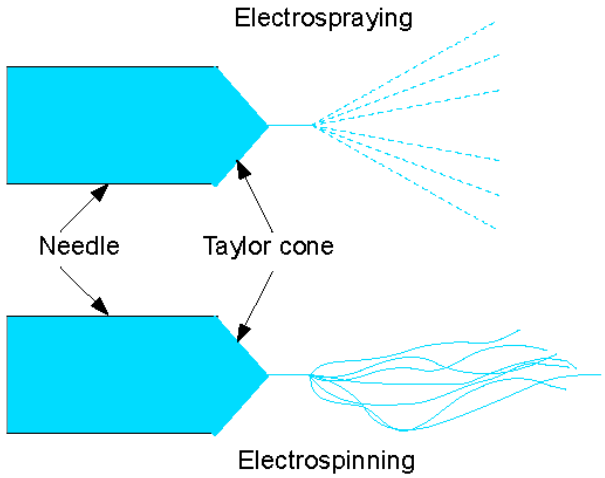

Figure 3.2: Different jet under electrospraying and electrospinning process.

Sir Geoffrey Taylor in 1964 theoretically derived equation to describe the shape of the liquid based on two assumptions: (1) Taylor cone has an equipotential surface and (2) Taylor cone is in stable state. In order to meet these two assumptions, the distance to the apex of the Taylor cone R shouldn't affect the value of the surface voltage V and the electric field should have azimuthal symmetry to balance the surface tension. The final solution is:

$$V = V_0 + AR^{\frac{1}{2}}P_{\frac{1}{2}}(cos\theta_0) \quad (5)$$

where V_0 is the voltage when R=0, A is a given value, and $P_{\frac{1}{2}}(cos\theta_0)$ is the Legendre polynomial of order $\frac{1}{2}$. In order to get an equipotential surface, V should be equal to V_0, that means $P_{\frac{1}{2}}(cos\theta_0)$ should be zero. Between 0° and 180°, 130.7099° is the only value of θ_0 that can make $P_{\frac{1}{2}}(cos\theta_0)$ equal 0. The Taylor angle is then calculated to be 180° - 130.7099° ≈ 49.3°. The Taylor angle is a semi-vertical angel, and the whole angle should be 98.6° [38].

3.1. Controlling Parameters in electrospraying

The electrosprayed nanoparticles and electrospun nanofibers are affected by many parameters that can be classified into three groups [34] [39]:

- Solution (or melt) properties: such as solution concentration, viscosity, volatility, vapor pressure, conductivity, surface tension, and the polymer molecular weight.

- Process variables: such as electrospraying voltage, the distance between the tip of needle and the collector, electrospraying/electrospinning time, and flow rates.

- Environment: such as the ambient temperature and humidity.

Usually environment is kept stable, and solution (or melt) properties and process variables are adjusted to have the desirable result.

4. Sensor Fabrication

4.1. Electrode Design and Patterning

MEMS are becoming more and more popular due to their several advantages: such as small size, low cost, low power consumption, and integration [40]. Interdigitated electrodes (IDEs) using micro fabrication technology are designed and fabricated for the humidity sensor. The interdigitated structure (see Figure 4.1) offers many advantages:

- It can increase the contact area between the electrodes and sensing material, which can improve the sensitivity of humidity sensor.
- It has a simple structure which can decrease the fabrication complexity and cost.
- It provides a relatively planar surface (e.g., 200 nm of roughness). The low aspect ratio of the structure could make the future fabrication steps simpler, especially during lithography process.

Six IDEs with different parameters were designed at first. The six IDEs are named **A**, **B**, **C**, **D**, **E**, and **F** as shown in Figure 4.2. All IDEs are square with length 5000 µm by 5000 µm. The parameters are listed in Table 4.1:

Table 4.1. Different parameters of six IDEs

IDE	Width of fingers (µm)	Gap between two fingers (µm)	Number of fingers
A	10	20	167
B	10	10	251
C	10	40	101
D	20	20	125
E	20	10	167
F	20	40	83

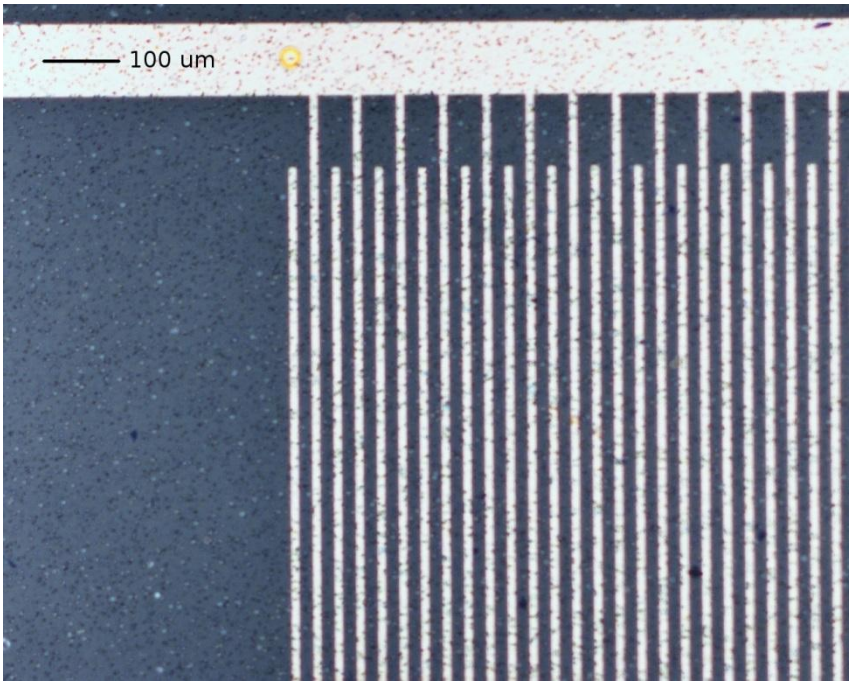

Figure 4.1: Close-up view of the electrodes coated with nanoparticles under microscope.

After fabrication, devices **B** and **E** always had a “short circuit”. **B** and **E** have 10 µm gaps in common which should be the reason for the failure. Among the rest of the four IDEs, **A** has the most fingers which translated into the most surface area. **A** also shows a good sensitivity between all the IDEs, so IDE **A** is picked to be used for the humidity sensor.

The material for IDE was gold and chromium first. Gold is used frequently in microfabrication and can be soldered to for electrical connections. However, gold is also sputtered during the reactive ion etching (RIE) step for etching polyimide film, which is used as the sensing material. On the other hand, Gold is also expensive, which will increase the fabrication cost. For this reason, aluminum was used as the material of IDE. Al is not etched during RIE step, but the adhesion between Al and solder material is not good. Therefore, silver conductive epoxy was used to bond wire on Al pads. Silver conductive epoxy is an electronic epoxy with good electrical and thermal conductivities.

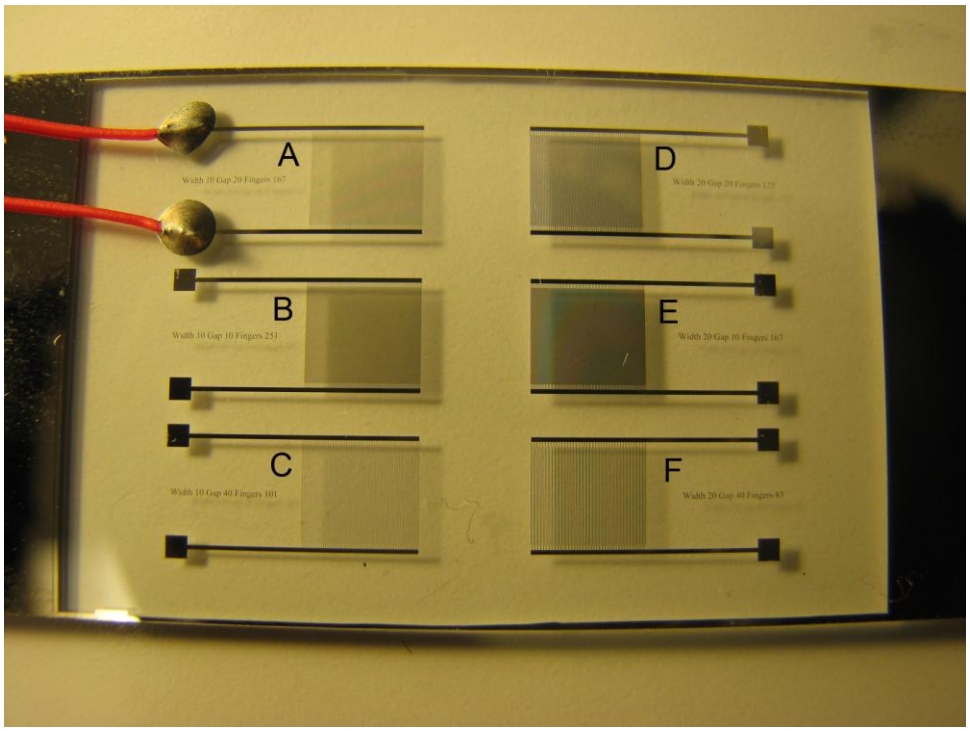

Figure 4.2: Interdigitated aluminum electrodes fabricated on a glass substrate.

The IDEs were fabricated in cleanroom. The fabrication steps are shown below (see Figure 4.3):

RCA SC-1 Clean

Glass slides are hydrated in DI water. 1000 mL DI H_2O is then poured in the container and heated to 80°C. 200 mL NH_4OH (30%) and 200 mL H_2O_2 are added to the container until the temperature is stabled around 80°C. Glass slides are then placed in the container for 10 minutes and rinsed in running DI water more than 3 minutes afterwards.

Sputtering Al

A 200 nm thick Al is sputtered on top of the glass substrate.

Spin-on Photoresist

S1813 positive photoresist (PR) is spun on top of Al at a speed of 3000 rpm for 30 seconds.

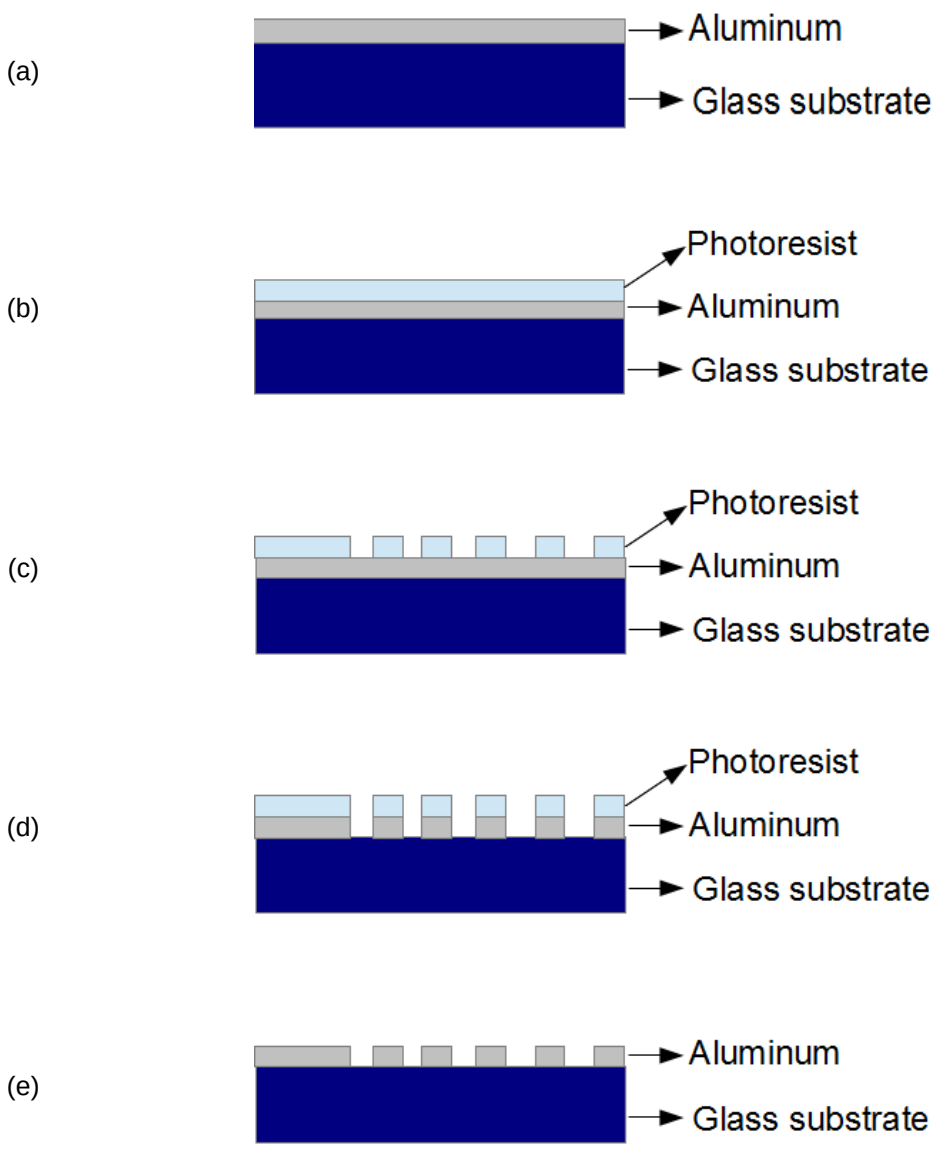

Figure 4.3: IDE fabrication steps: (a) sputtering Al, (b) spin-on PR, (c) lithography, (d) etching Al, (e) remove PR.

Lithography

The sample is put on a hot plate for 1 minute at 115°C before placing it under the mask and exposure to UV light for 10 seconds. MF-319 is used to develop PR on top of

the sample. The sample is then put on hot plate for 1 minute and 10 seconds at 115°C to hard bake the PR.

Al Etch

Al etchant is used to etch Al around 2 minutes.

Remove PR

Acetone is used to clean the PR left on top of the sample.

4.2. Polyimide Deposition

Polyimide (PI) PI-2555 has been used as the sensing material due to its low hysteresis, chemical stability, and stability over a wide range of temperature. PI exhibits good sensitivity to humidity changes [41]. PI also shows good stability when exposed to most chemicals, which has led to its widespread application in electronics industry as a protective layer [42]. The humidity sensor is realized by putting a PI layer on top of the IDEs on a glass substrate. Absorption of the water vapor changes the PI's dielectric constant which is sensed as a change in the capacitance of the interdigitated structure underneath.

Two methods were used to produce a layer of PI on top of the interdigitated structure. The first method is the traditional spinning, which can be done by spinning the PI inside the cleanroom. The other technique is electrospraying of PI.

4.2.1. Spin-on Polyimide

The first sets of devices were fabricated using a spun-on PI film on top of the IDEs. The thickness of the spun-on PI layers is uniform across the samples. PI should be stored in a fridge. Before use, it needs to be allowed to reach room temperature. The fabrication steps for spinning on a PI film are shown below (see Figure 4.4):

Spinning on PI

PI is poured at the center of the IDEs samples. In the beginning, PI is spun at 500 rpm for 30 seconds, and then the rate is quickly increased to 5000 rpm and spun for another 30 seconds.

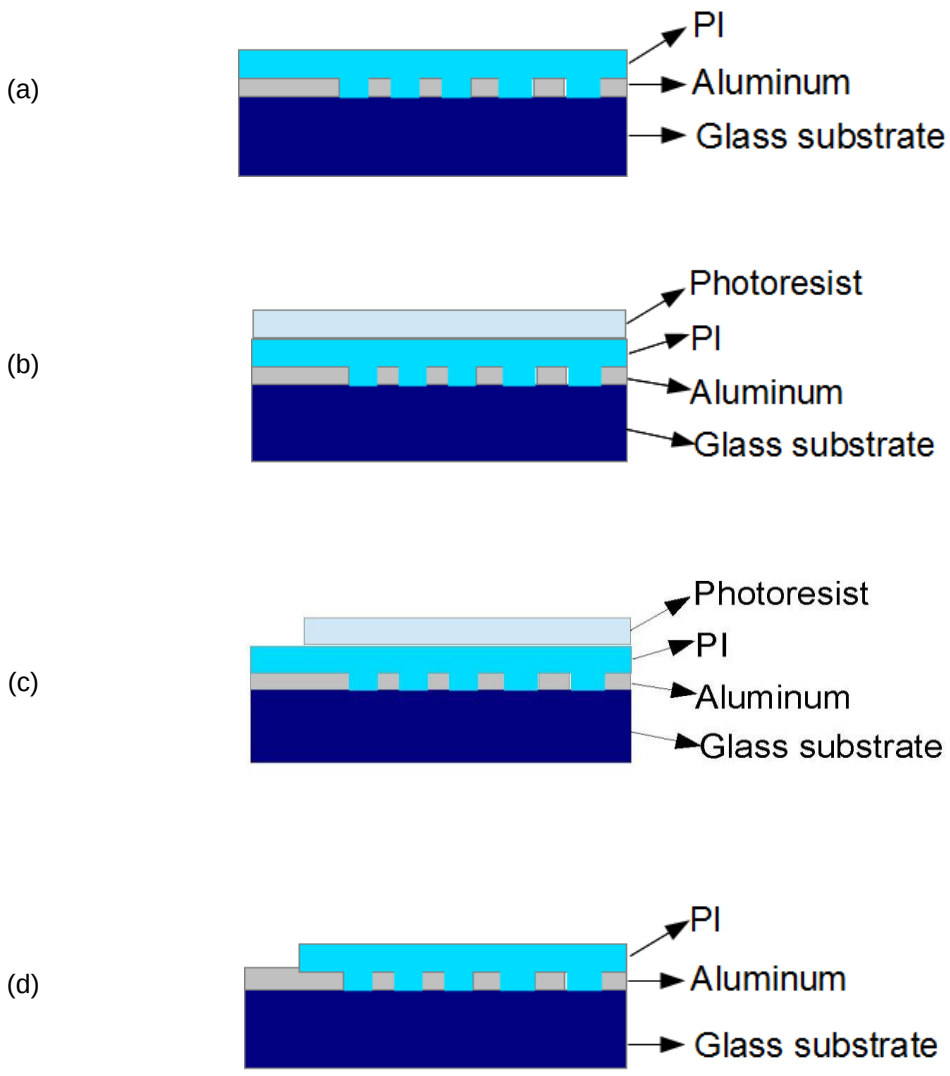

Figure 4.4: Fabrication steps of spin-on PI: (a) spinning on PI, (b) spinning on PR, (c) lithography, (d) patterning.

Spinning on PR

The sample is put on hot plate for 3 minutes at 100°C, and then another 3 minutes at 150°C for soft bake. The temperature is increased from 150°C to 200°C in 13 minutes with 4°C steps per minute to cure the film. The samples are kept at 200°C for 40 minutes.

Photoresist S1813 was spun on top of the PI at a speed of 3000 rpm for 30 seconds.

Lithography

The sample is put on top of the hot plate for 1 minute at 115°C before being put under the mask aligner and exposure to UV light for 10 seconds. MF-319 was used to develop the PR on top of the PI

Patterning

The RIE process is used for patterning the PI film and removing it from the contact pads. The parameters of this process are:

- Process pressure: 300 mTorr
- CF_4 flow: 10 sccm
- O_2 flow: 50 sccm
- Forward power: 250W
- Time: 5 minutes

Figure 4.5 shows the fabricated spun-on PI. Although spin-on method can make a uniform PI, there are still some disadvantages:

- PI shows good stability when exposed to most chemicals, which makes the process of patterning the PI complicated. Therefore, the number of the fabrication steps is increased significantly.
- After changing the IDEs material from gold chromium to aluminum, the IDEs are not etched during the RIE process. However, in the RIE process, PR is also etched. Sometimes the PI underneath is also etched completely during the RIE process which makes it hard to control the thickness of PI.

- The uniform PI film has a relatively small surface area. A patterned surface provides more area for the absorption of water vapor and increases the sensitivity of the sensor while reducing its response time.

- The fabrication process for spin-on method needs to be completed in a cleanroom.

To overcome these shortcomings, another method, electrospraying of PI, is proposed.

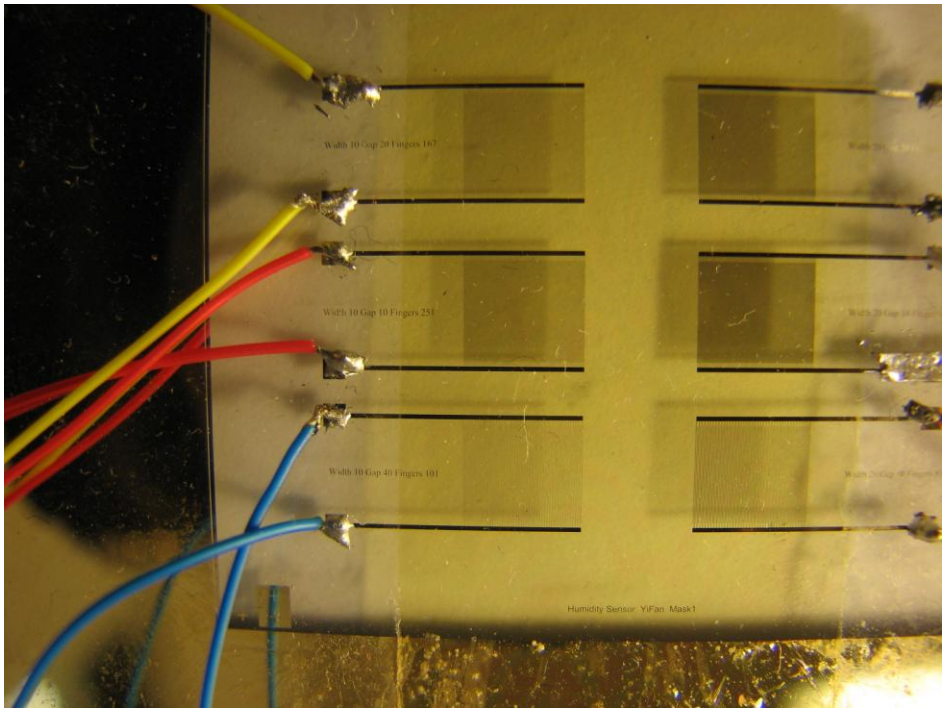

Figure 4.5: IDEs with spin-on uniform PI on top.

4.2.2. Electrosprayed Polyimide

Figure 4.6 shows the electrospraying set-up used in this thesis. Electrospraying employs a high voltage to build a large electric field between the tip of a metallic needle and a collector. The liquid in the syringe is slowly pumped out and form a Taylor cone at the tip of the metallic needle in the electric field. It is then jetted and deposited on the surface of the collector. The fabrication steps for electrospraying are shown below:

Electrospraying

PI nanoparticles are electrosprayed on the collector under controlled parameters. The sample with PI nanoparticles is then put on top of the hot plate and baked for 1 hour at 100°C (see Figure 4.7).

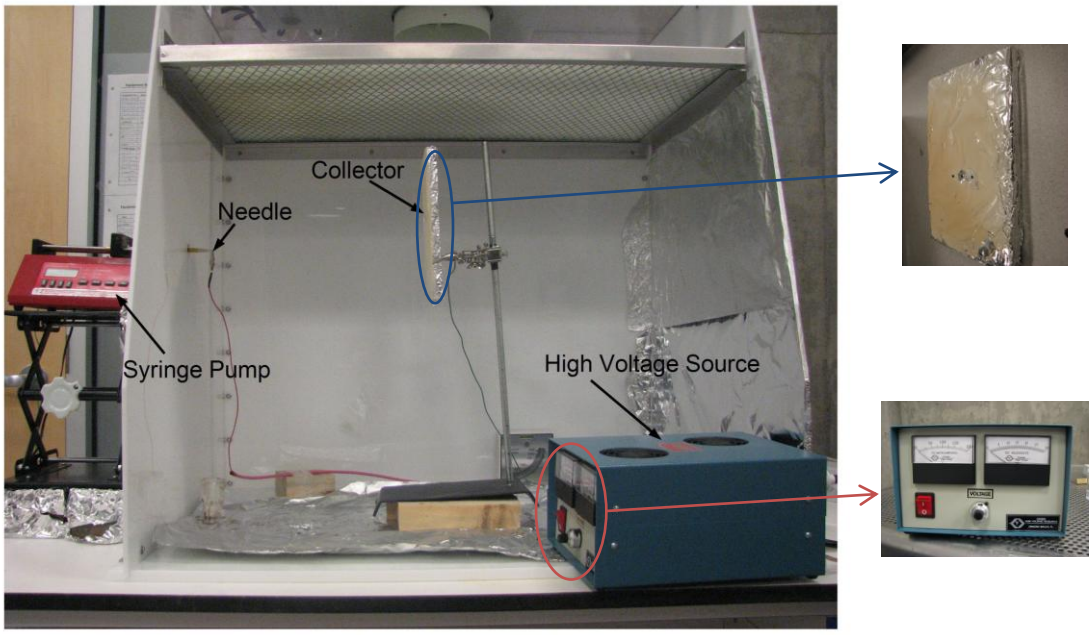

Figure 4.6: Electrospraying set-up.

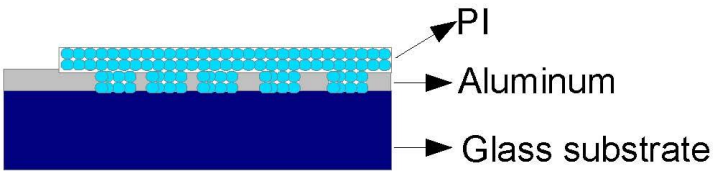

Figure 4.7: Fabrication step of electrospraying PI on IDEs is simple and completed in one step.

A shadow mask is used to protect pads during the PI film deposition. It is easy to see that electrospraying PI has less fabrication steps than spin-on PI. The fabrication steps comparison is shown in Figure 4.8. The comparison between the experimental results for the spin-on PI and electrospraying PI processes will be discussed in Chapter 6.

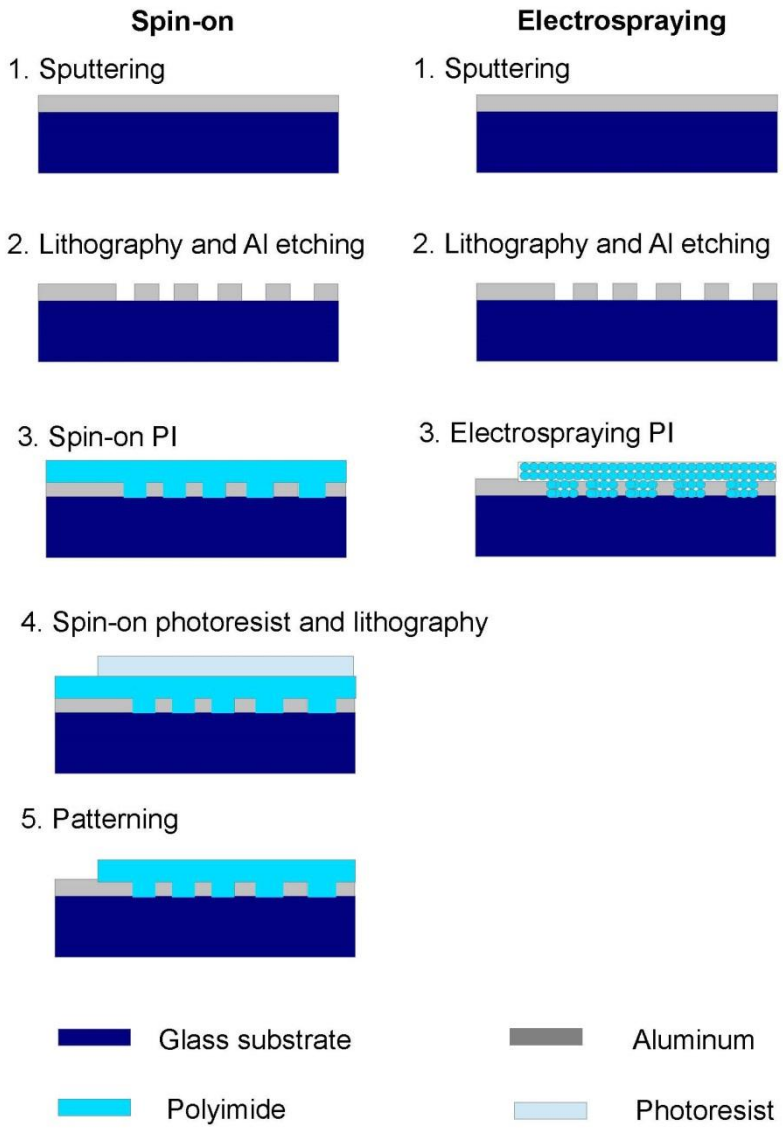

Figure 4.8: Comparisons between the fabrication steps for the spin-on PI and electrospraying PI processes.

The properties of the electrosprayed PI nanoparticles are determined by many parameters. The parameters under control are PI properties, curing temperature, electrospraying voltage, the distance between the tip of needle and the collector,

electrospraying time, and flow rates. Optimizing of these parameters strongly affects the quality of the film, and therefore, the sensitivity of the sensor.

(a)

(b)

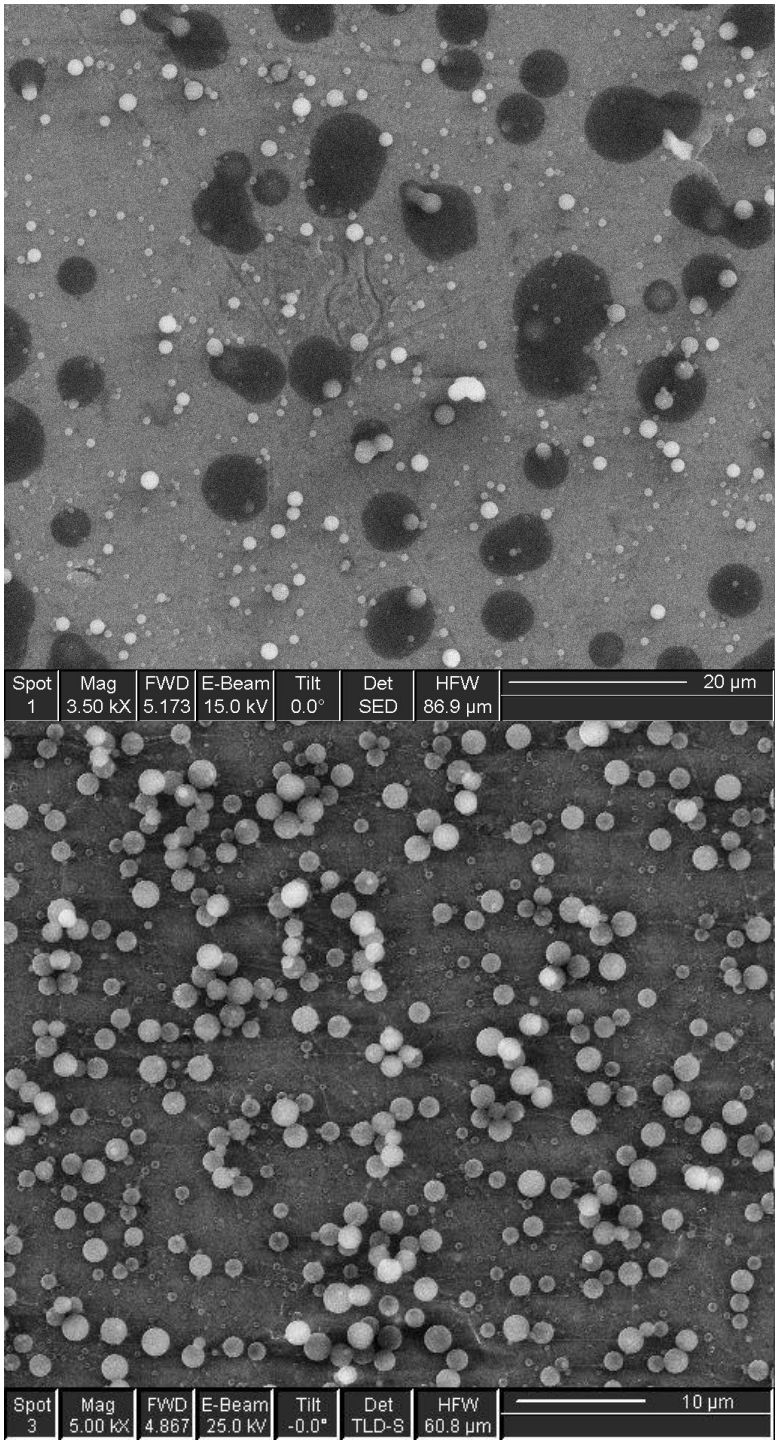

Figure 4.9: SEM images of (a) PI-2611 and (b) PI-2555 with 15/30 kV/cm electrosprayed for 30 min.

PI-2611 was initially used as the sensing material. PI-2611 is a low moisture uptake, and low stress polyimide. The PI-2611 was mixed with thinner before using for electrospraying. The PI-2611 thinner used was prepared through mixing N-Methyl-2-Pyrrolidone (NMP) with acetone at the ratio of 1:1. PI-2611 also needs high curing temperature up to 350°C. After a long time research with different concentration of PI-2611, we could not reliably produce nanoparticles with electrospinning/electrospraying of PI-2611. Therefore, PI-2555 was chosen to be used as the sensing material. The curing temperature of PI-2555 is lower and the PI-2555 is thinner compared to PI-2611. Electrospraying PI-2555 led to better nanoparticle formation results as verified through scanning electron microscope (SEM) (see Figure 4.9).

By increasing the electrospraying time, more nanoparticles and nanofibers can be deposited (see Figure 4.10). The PI nanoparticles are electrosprayed on the top of a piece of Aluminum foil. It was found that after long electrospraying times; nanoparticles may not stick on the surface of the aluminum. When the sample with electrosprayed PI nanoparticles was inspected under SEM, the electron beam would charge up the

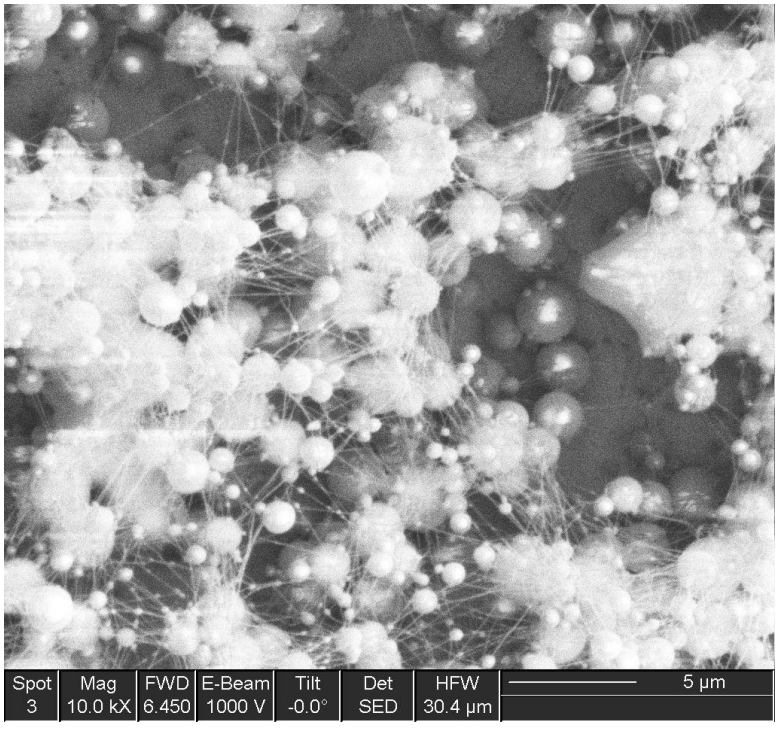

Figure 4.10: PI-2555 with 15/30 kV/cm electrosprayed for 120 min under SEM.

(a)

(b)

(c)

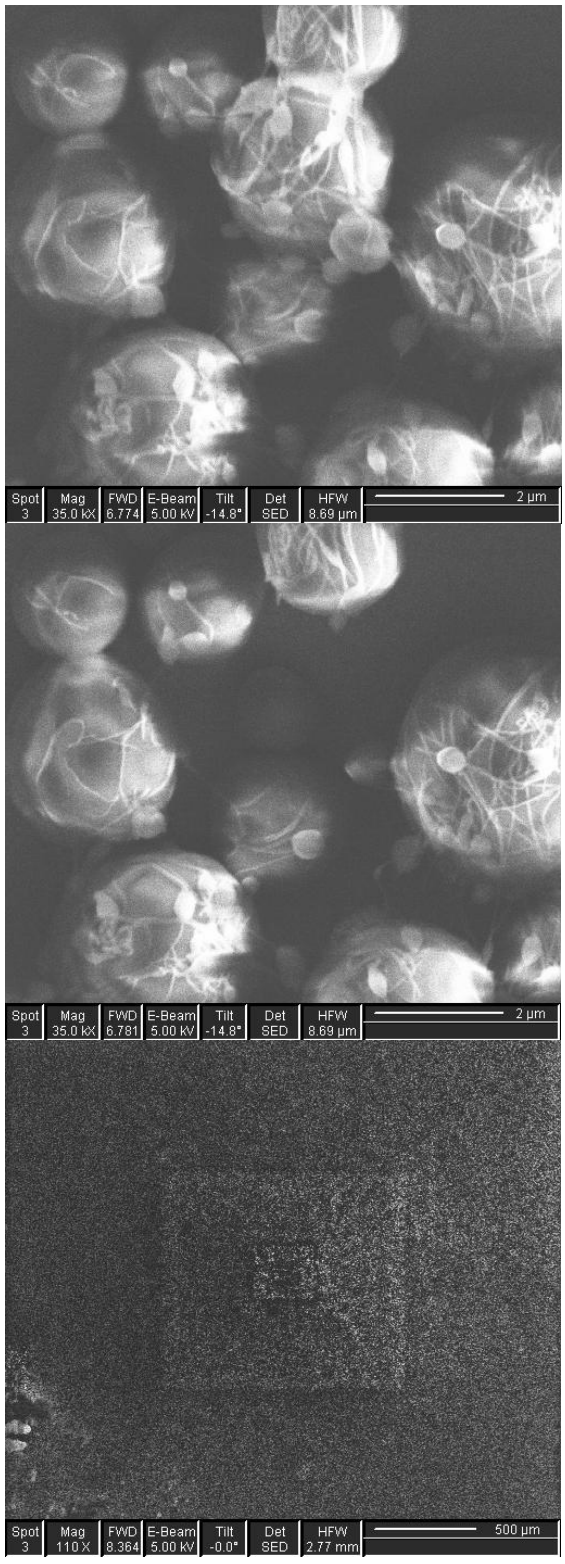

Figure 4.11: PI-2555 electrosprayed for 60min under SEM: (a) short time under SEM exposure, (b) long time under SEM exposure, (c) forms a figure shown in small magnitude.

nanoparticles. The nanoparticles which were not on the Al surface or tightly bonded by other nanoparticles were moved due to the charging. Figure 4.11 (a) (b) displays a case where a single nanoparticle disappeared from the picture due to charging. Figure 4.11 (c) shows a figure formed with SEM.

The curing temperature for electrospraying was set at 200°C similar to the spin-on method. But the experimental results showed that it resulted in a totally non-linear sensor behavior. Therefore, the curing temperature was set to 100°C, 150°C (**E15** in table 4.2), and 200°C (**E16** in table 4.2) to find out the best curing temperature. It was found that 100°C resulted in the best sensing performance and was selected for future samples.

Other parameters of electrospraying were also studied during this research. It was found that the distance between the tip of needle and the collector should be shorter than the height between the collector and the ground so that the PI nanoparticles do not hit on the ground instead of the collector; the electrospraying time should be long enough to produce enough PI nanoparticles.

All the sensors fabricated and tested are listed below (“Distance” shown in the table 4.2 is the distance between the tip of the needle and the collector):

Table 4.2. A list of all the fabricated and tested sensors

Sensor	Spin rate (rpm) and time (seconds)	Thickness (µm)	Flow rate (ml/hr)	Voltage (kV)	Distance (cm)	Electrospraying time (minutes)	Curing temperature (°C) and time	Notes
B1								Bare sample (no PI on top of IDEs)
S1	500 rpm for 30 sec plus 5000 rpm for 30 sec	1					100 °C and 150 °C for 3 min each; ramp to 200 °C in 13 min, and then cured at 200 °C for 40 min	
S2	500 rpm for 30 sec plus 4000 rpm for 30 sec	1.2						
E1			0.1	10	28	5	100 °C for one hour	
E2			0.1	10	28	10		
E3			0.1	10	28	15		
E4			0.1	15	30	30		
E5			0.1	15	30	60		
E6			0.1	15	30	90		
E7			0.1	6.7	8	10		
E8			0.1	13.3	45.5	10		

Table 4.2. Continued

Sensor	Spin rate (rpm) and time (seconds)	Thickness (µm)	Flow rate (ml/hr)	Voltage (kV)	Distance (cm)	Electrospraying time (minutes)	Curing temperature (°C) and time	Notes
E9			0.1	25	30	30		
E10			0.11	9.6	21	10	100 °C for one hour	
E11			0.11	9.6	21	14		
E12			0.11	10.1	28	10		
E13			0.1	25	30	20		Less nanoparticles
E14			0.11	10.1	28	10	Not cured	Non-linear results
E15			0.11	10.1	28	10	150 °C for one hour	Experimental results are not good
E16			0.11	10.1	28	10	200 °C for one hour	
E17			9	13	44	12	100 °C for one hour	
E18			9	13.9	44	8		
E19			0.5	15	12	5		

5. Interface Electronics

There are several methods for measuring capacitance. A straight forward method is using a capacitance meter. At low RH, the capacitance meter works well with the humidity sensor (typical capacitances are between 20 to 40 pF under 60% RH). But when testing at higher RH, the measured capacitance value has significant errors (e.g., the capacitance will increase from 40 pF to around 1000 pF after 60% RH). When the RH is increasing, the PI on top of the IDEs will absorb more vapor so as to increase the capacitance of the humidity sensor. However, the conductance will also increase as the RH increases. A simple capacitance meter has a difficult time separating the capacitive and resistive currents at the same time, which leads to the error in capacitance values. In order to solve this problem, two kinds of circuits were designed which are introduced in the following sections to measure the capacitance of the humidity sensor.

5.1. Capacitive Sensing Circuit

The capacitive sensing circuit (C-V circuit) consists of four main blocks (see Figure 5.1): differential reference signal generator, capacitance to voltage converter (C-V converter); a synchronous demodulator including a phase shifter and a switch; and a filter for converting the amplitude of demodulated signal into a DC signal. The test capacitor is placed between electrodes *Electrode*+ and *Electrodemid* connectors (see Figure 5.2). The reference capacitor is connected to the *Electrode*- and *Electrodemid* connectors. The circuit works by comparing the currents through the test and reference capacitors.

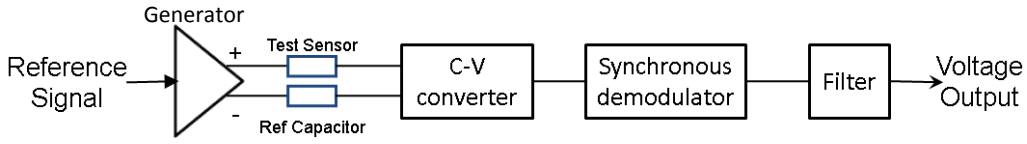

Figure 5.1: The block diagram of the C-V circuit.

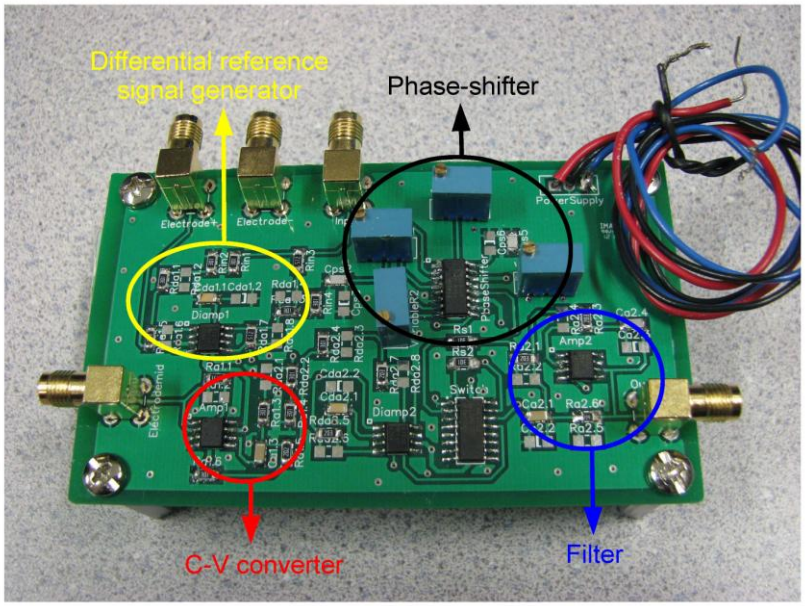

Figure 5.2: Capacitive sensing circuit.

A. Differential Reference Signal Generator

The reference signal from the function generator is a 2 V, 250 kHz sinusoidal signal. The reference signal goes through the differential reference signal generator and generates two inverted signals, which goes to the test sensor and reference sensor.

B. C-V converter

The C-V converter block translates the changes in capacitance, the capacitance of the reference capacitor minus the capacitance of the test sensor, to a voltage signal using a trans-impedance amplifier [43]. The general expression of the output voltage is shown in equation (6):

$$V_{C-V} = 0.5(C_2 - C_1)\sin\left(\pi t + \frac{\pi}{2}\right) \quad (6)$$

where C_1 and C_2 are the reference capacitor and the test capacitor, respectively (see Figure 5.3). As can be seen, there is a 90-degree phase shift between the voltage produced from the C-V convertor and the reference signal $V_{in}(t) = 2\sin(\pi t)$.

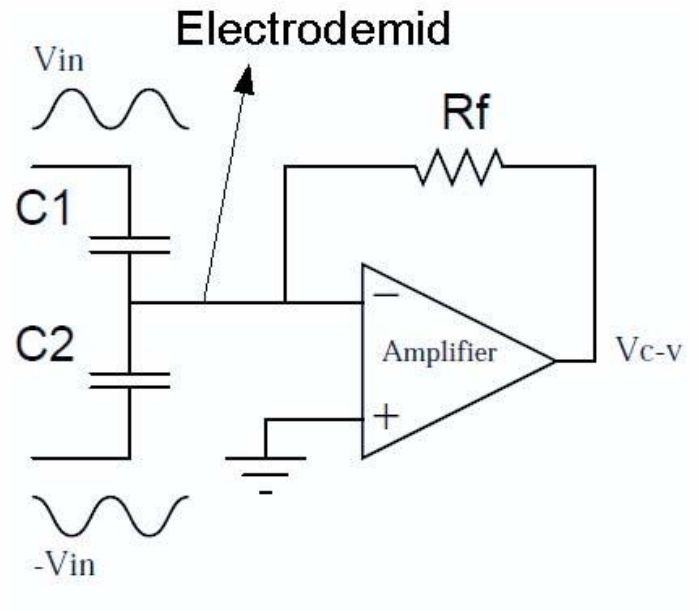

Figure 5.3: Simplified model for the input stage made with a trans-impedance amplifier [43] © [2012] IEEE. Reprinted, with permission, from [F. Aezinia, Y. Wang and B. Bahreyni, "Three dimensional touchless tracking of objects using integrated capacitive sensors," IEEE Transactions onConsumer Electronics, August 2012].

C. Synchronous Demodulator

The block includes 90° and 270° phase shifters and switches. As shown in Figure 5.4 (a), two switches are controlled by two square-wave signals provided by the 90°/270° phase shifter stages to offset the initial phase shift of the signal from C-V converter [43]. Phase tuning can be performed by simple circuit made of comparators and RC delay circuits as shown in Figure 5.4 (b). The output voltage, $V_{i-Filter}(t)$, is a full-wave rectified signal.

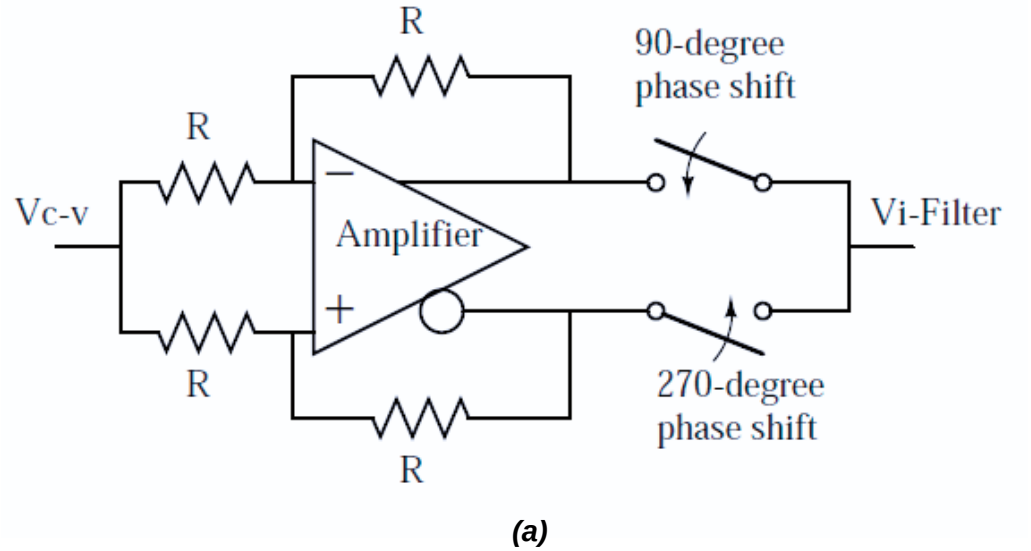

(a)

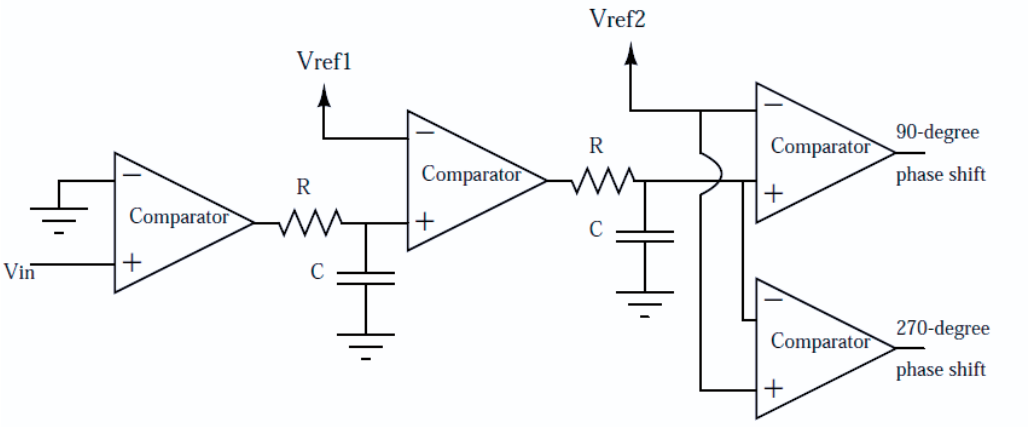

(b)

Figure 5.4: Schematic of (a) differential amplifier with demodulator switches, and (b) 90° and 270° phase shifter stage made of comparators and RC delay circuits [43] © [2012] IEEE. Reprinted, with permission, from [F. Aezinia, Y. Wang and B. Bahreyni, "Three dimensional touchless tracking of objects using integrated capacitive sensors," IEEE Transactions onConsumer Electronics, August 2012].

D. Filter

A Bessel low pass filter, which is the final block of the interface electronic structure, is used to extract the DC component of the signal (see Figure 5.5). Output of the low pass filter is a DC voltage which is proportional to the amplitude of the rectified signal $V_{i-Filter}(t)$ from the previous block. The output voltage can be converted to capacitance from:

$$V_{out} = 0.32(C_2 - C_1) \tag{7}$$

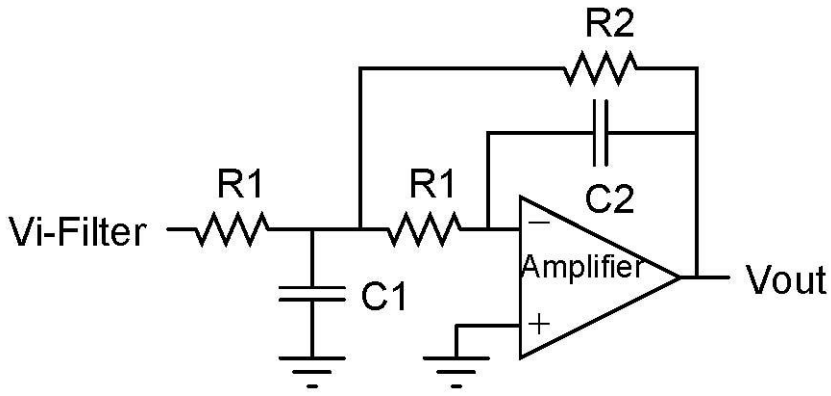

Figure 5.5: Bessel low pass filter which can convert the amplitude of demodulated signal into a DC signal.

As the RH changes, the capacitance of the humidity sensor will change. Because the reference capacitor value is fixed, the reference capacitance minus the humidity sensor capacitance will change by the same value as the humidity sensor capacitance. The output voltage change is related to the capacitance change between reference capacitor and humidity sensor. That is to say, the output voltage change is only related to the change of humidity sensor capacitance. When the capacitance of the humidity sensor increases, the output DC voltage will therefore change proportionally. As the output voltage is converted from capacitance not resistance, the voltage change can show only the change of the capacitance of the humidity sensor.

5.2. Oscillator Circuit

The oscillator circuit (C-F circuit) shares a similar idea with the C-V circuit. The C-F circuit converts the capacitance to frequency, which can also remove the effect of the resistance change of the humidity sensor. The C-F circuit is shown in Figure 5.6.

The circuit operation is as follows. Assume the output voltage V_{out} is positive at a moment. The feedback fraction $\beta = \frac{R_2}{R_1+R_2}$ is fed back to the non-inverting input (Q), and V_{out} is fed back to the inverting input (P). The voltage across the capacitor (V_P) rises exponentially as C is charged. At some point, V_P becomes larger than V_Q after a certain time which is related to CR_1. The op-amp will switch to negative rail ($V_{out} = V_{cc-}$) and the signal Q becomes negative. C discharges in the opposite direction and V_P will fall down until $V_P < V_Q$. The op-amp will switch to positive saturation ($V_{out} = V_{cc+}$) and the cycle repeats. The output voltage V_{out} is therefore a square wave as shown in Figure 5.7. The output frequency f can be converted to capacitance, C, of the humidity sensor from:

$$C = \frac{1}{f} \frac{1}{2\, R_3 \,\mathrm{Ln}\frac{2R_1 + R_2}{R_2}} \tag{8}$$

where R_1, R_2, and R_3 are the resistors on the C-F circuit.

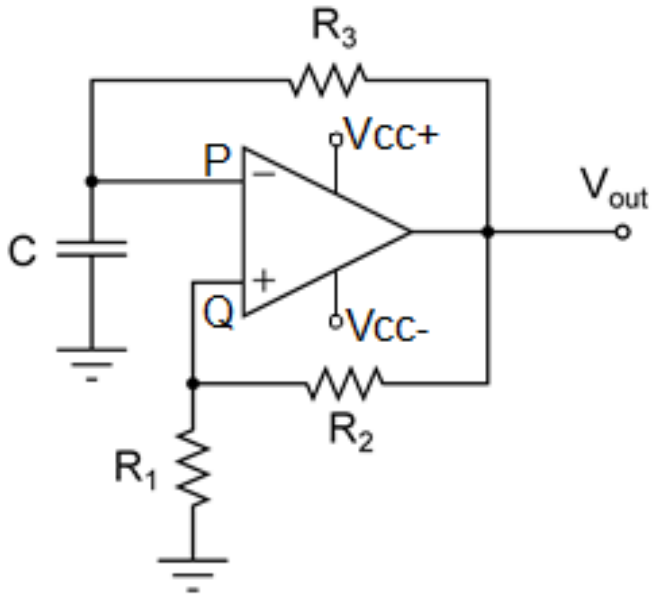

Figure 5.6: C-F circuit for converting capacitance to frequency.

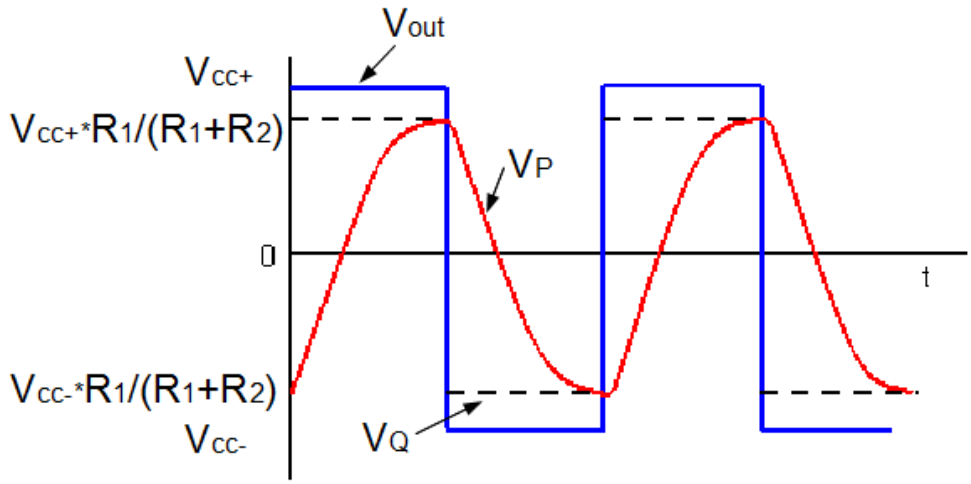

Figure 5.7: Waveform of the C-F circuit.

As can be seen, the time talked above for V_{out} to change from positive to negative (or from negative to positive) is related to C, which means the output frequency is related to C. The capacitive humidity sensor is placed as C in Figure 5.6. The output frequency will therefore change following the change of the capacitance of the humidity sensor, which in turn follows changes in RH.

6. Experimental Results

The aim of this thesis is to fabricate a capacitive humidity sensor with simple structure. Several methods were utilized and different equipment was used to improve the performance of the humidity sensor. The experimental results and comparison are discussed in the following sections.

The RH sensors are used in this chapter are list below (IDE A is used for all the sensors used in Chapter 6):

B1: bare sample (no PI on top of IDEs)

S1: spin rate and time: 500 rpm for 30 seconds plus 5000 rpm for 30 seconds, thickness: 1μm

E1 ~ E13 are listed in Table 6.1

Table 6.1. Electrosprayed RH sensor E1 ~ E13

Sensor	Electric field (kV/cm)	Electrospraying time (minutes)	Polyimide
E1	10/28	5	PI-2555
E2	10/28	10	
E3	10/28	15	
E4	15/30	30	
E5	15/30	60	
E6	15/30	90	
E7	6.7/8	10	
E8	13.3/45.5	10	
E9	25/30	30	
E10	9.6/21	10	PI-2611
E11	9.6/21	14	
E12	10.1/28	10	
E13	25/30	20	

The capacitance of the RH sensor C and the voltage V read from the humidity sensor HIH-4000-003 are measured by:

$$C = C_0 + \Delta C \tag{10}$$

$$V = V_0 + \Delta V \tag{11}$$

where C_0 is the capacitance of lowest RH, ΔC is the capacitance change, and V_0 is the output voltage of the reference sensor at lowest RH. For experimental results, C_0 and ΔC (V_0 and ΔV) are reported.

We waited at least 20 minutes between taking data points for all of the experiments. Relative humidity is a strong function of temperature. Ideally, one needs to use a humidity chamber with both temperature and humidity control to test an RH sensor. However, due to the limitation of our setup, all of the experiments were conducted at room temperature..

6.1. Measurements with Spin-on Thin Films

Spin-on technique has been traditionally used to produce uniform thin films of PI. The fabrication steps and disadvantages of spin-on method were mentioned in Chapter 4. The experimental results with DI water (Deionized water) are better than the experimental results with tap water, which is discussed in section 4.

The experiment set-up is shown in Figure 6.1. Nitrogen gas flows into two lines from the tank. One line is connected to the flow meter 1 (FM1) and then to the chamber; the other line is connected to a DI water reservoir, passing flow meter 2 (FM2), and then to the chamber. The flow rates are set to the minimums possible with our flow meters so that we have near saturation level RH in DI water reservoir. The humidity in the chamber can be controlled by controlling the rate of nitrogen that flows through FM1 and FM2. A reference humidity sensor (HIH-4000-003) and a test sensor (i.e., the capacitive RH sensor) are placed inside the chamber. The reference sensor which is used to monitor the RH level inside the chamber is connected to a multimeter and the test sensor is connected to a LCR meter. Both multimeter and LCR meter are connected to a PC which saves all the data using a custom LabView program.

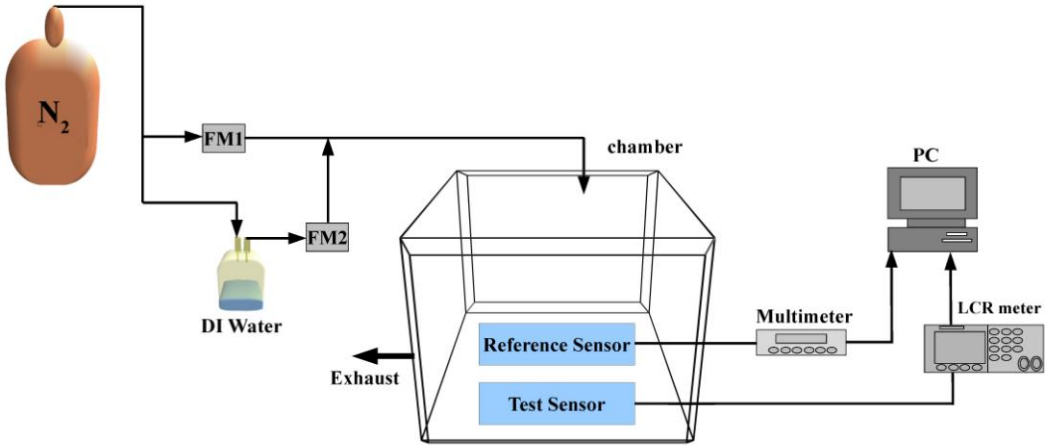

Figure 6.1: Measurement setup for LCR meter.

Agilent E4980A LCR meter was used for reading the capacitance of the test sensor, which provides susceptance, B, for a complex impedance. Capacitance C can be then calculated from:

$$C = \frac{B}{2\pi f} \tag{12}$$

where f is the frequency of measurement as set on the LCR meter (10 kHz or 100 kHz).

Figure 6.2 shows two experimental results of RH sensor **S1** with two test methods: the results shown in figure (a) and (b) are measured with the C-F circuit and LCR meter, respectively. Both (a) and (b) exhibit highly nonlinear behavior for capacitances values after 60% RH in figure (a) and (b). The nonlinear result is caused by the condensation which led to increasing both conduction and capacitance currents.

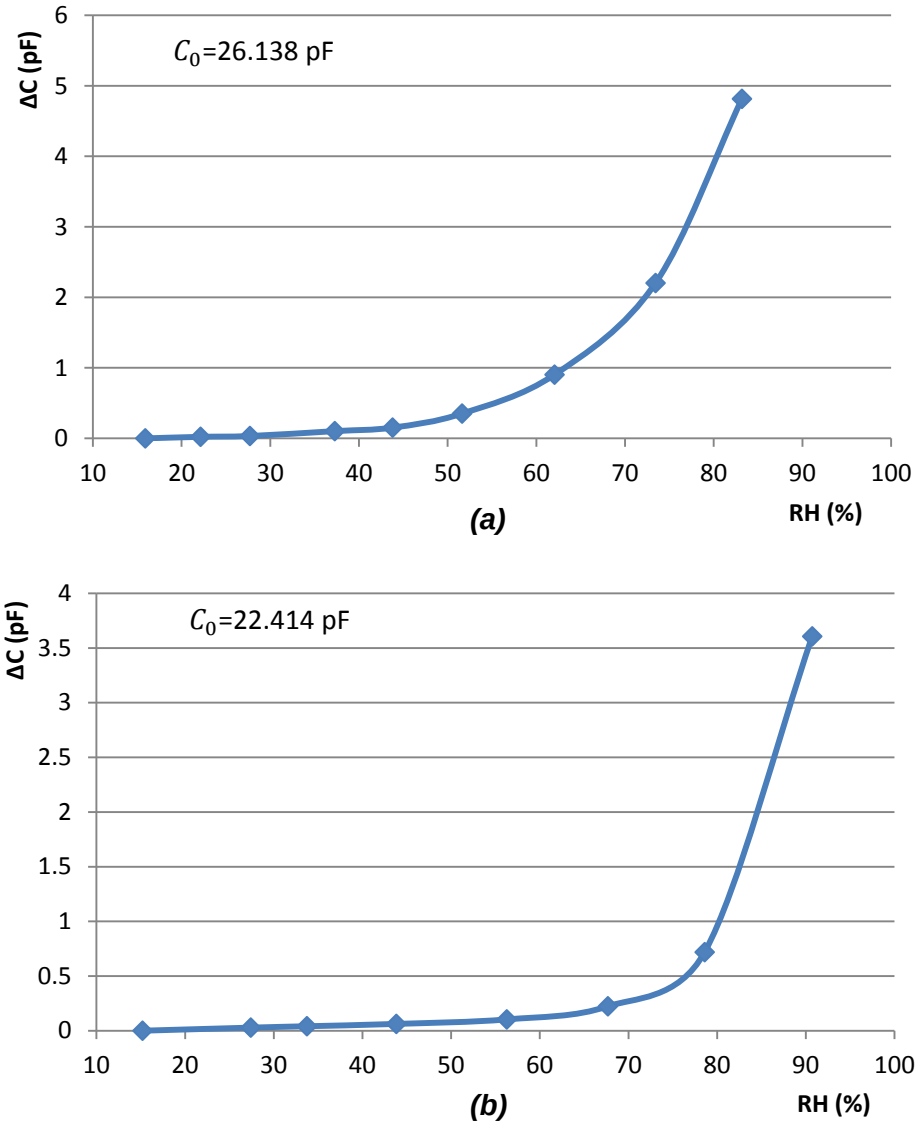

Figure 6.2: Experimental results of sensor S1 with (a) C-F circuit (from 16% to 83% RH), (b) LCR meter (from 18% to 91% RH).

Figure 6.3 and Figure 6.2 show experimental results for different humidity range. The experimental result obtained by LCR meter shows a better linearity at low RH. It can also be seen that the C_0 detected by oscillator circuit is larger than C_0 detected by LCR meter. This is due to the parasitic capacitances on the oscillator board as well as the input capacitance of the OpAmp used to realize the circuit.

The method with LCR meter has more accuracy and requires less equipment compared to the method using C-F circuit. It is also easier to calculate the capacitance of the test sensor with LCR meter. Spin-on method has some disadvantages compared to the electrospraying method which is talked about in the Chapter 4. The experimental results of uniform thin films show non-linearity due to the increase conduction current at high humidity range. The experimental results with electrospraying method are discussed in next section.

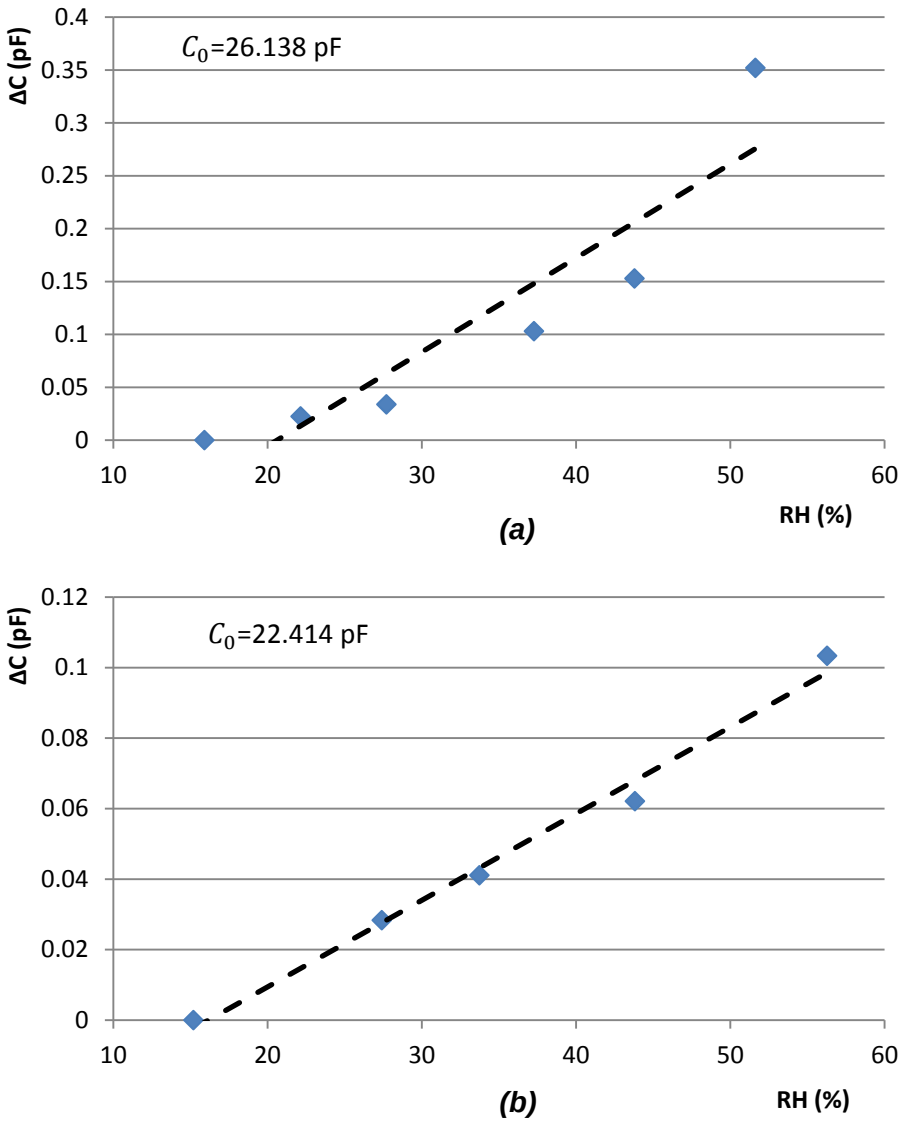

Figure 6.3: Experimental results of sensor S1 with (a) C-F circuit (from 15% to 51% RH); (b) LCR meter (from 15% to 56% RH).

6.2. Measurements with electrosprayed layers

There are many parameters which affect the results with electrosprayed layers (discussed in Chapter 3). The effect of the process variables will be discussed in this section.

6.2.1. Effect of Electrospraying Time

Different PI film thicknesses can be produced with different electrospraying time, which will affect the sensor performance. Figure 6.4 shows experimental results of RH sensors **E1**, **E2**, and **E3** from 10% to 90% RH. The only different parameter among these three RH sensors is the electrospraying time. The sensor with 5 minutes electrospraying time has 20 times more capacitance change than the one prepared with 15 minutes electrospraying time. The linearity of all sensors is compromised after 60% RH. The discussion will focus on experimental results below 60% RH.

Figure 6.5 compares RH sensor **E1**, **E2**, and **E3** from 10% to 63% RH. As shown in Figure 6.5, the film deposited through a 10 minutes of electrospraying shows the best linearity. 5 minutes electrospraying time shows the worst linearity but the highest capacitance change. The poor linearity may be caused by the short electrospraying time which leaves the sensor more prone to increase in conduction current; i.e., there was not enough PI on top of IDE with short electrospraying time.

RH sensors **E4**, **E5**, and **E6** are shown in Figure 6.6 to indicate the effect of the electrospraying time. The electrospraying times were changed to 30 minutes, 60 minutes, and 90 minutes which are much longer than the ones for sensors **E1** to **E3** (see Figure 6.5). **E6** has the longest electrospraying time while **E3** has the shortest electrospraying time. As it can be seen, **E6** has the best linearity and sensitivity among these three results while **E3** has the worst linearity and sensitivity. The conclusion from this experiment was that longer electrospraying times result in higher linearity and sensitivity. However, an upper bound for spraying time or film thickness was not found.

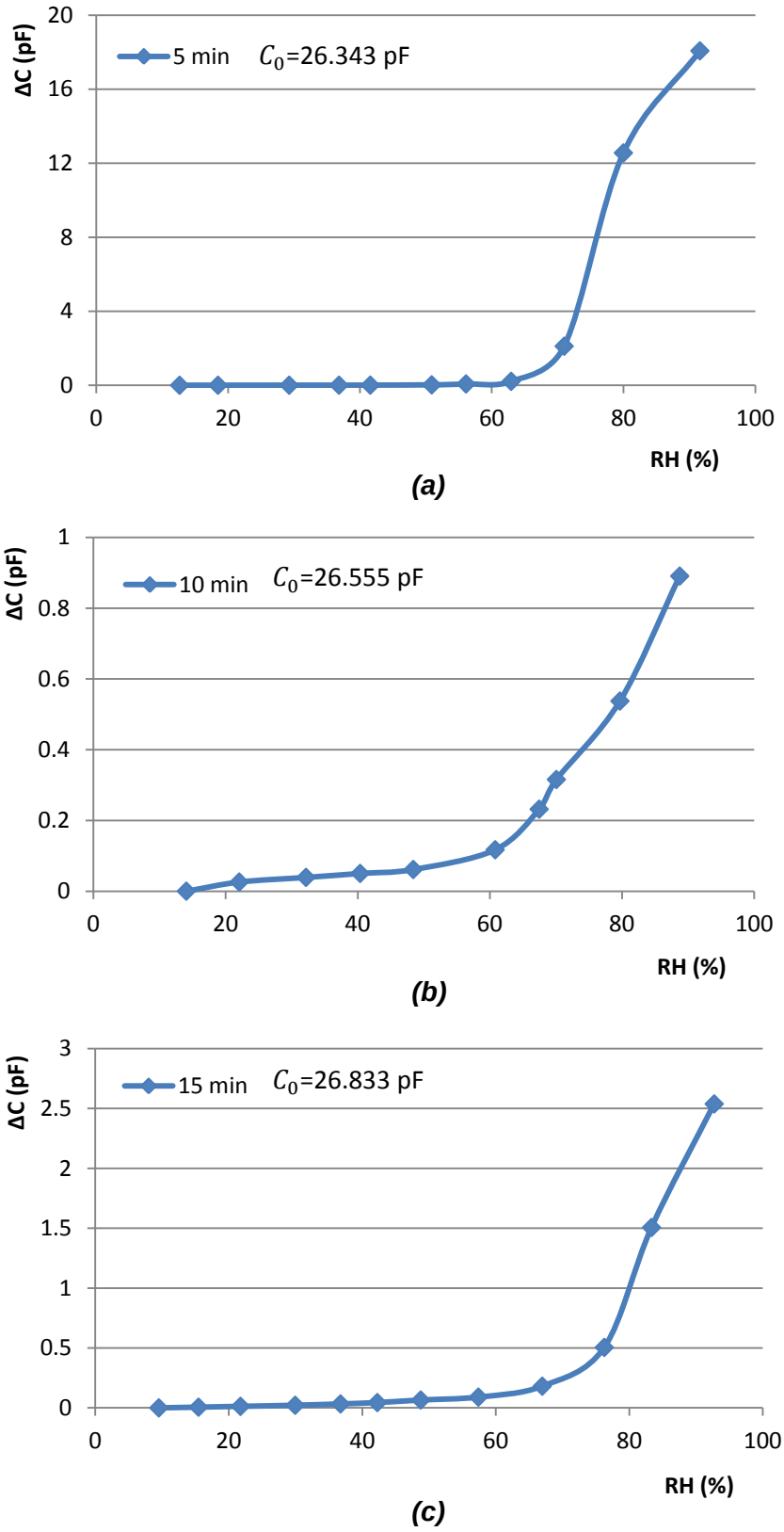

Figure 6.4: Experimental results of sensors: (a) E1; (b) E2; (c) E3 from 10% to around 90% RH (detected by oscillator circuit).

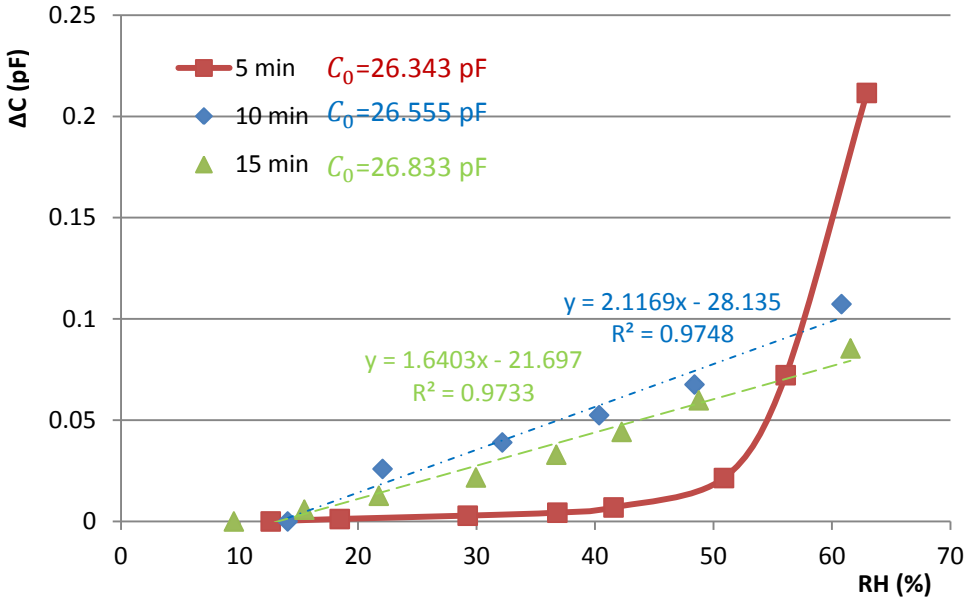

Figure 6.5: Experimental results of sensors E1, E2, and E3 from 10% to 63% RH (detected by oscillator circuit).

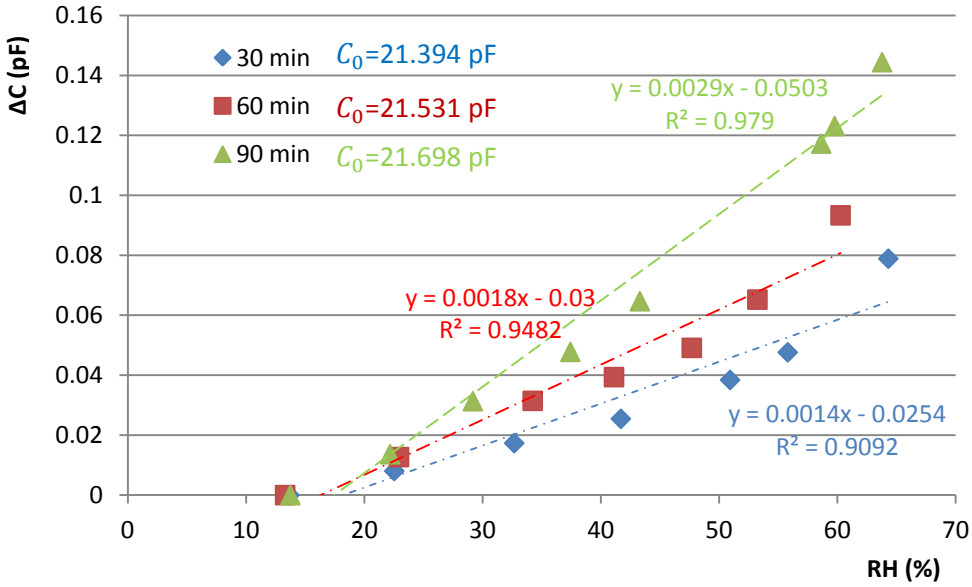

Figure 6.6: Effect of electrospraying time indicated by the experimental results of sensors E4, E5, and E6 from 13% to 64% RH (detected by LCR meter).

6.2.2. *Effect of Electric Field*

Electric field is another parameter which can affect the sensor performance. Electrospraying voltage and distance were modified to improve performance. RH sensors **E2**, **E7**, and **E8** are compared in Figure 6.7 to indicate the effect of electric field.

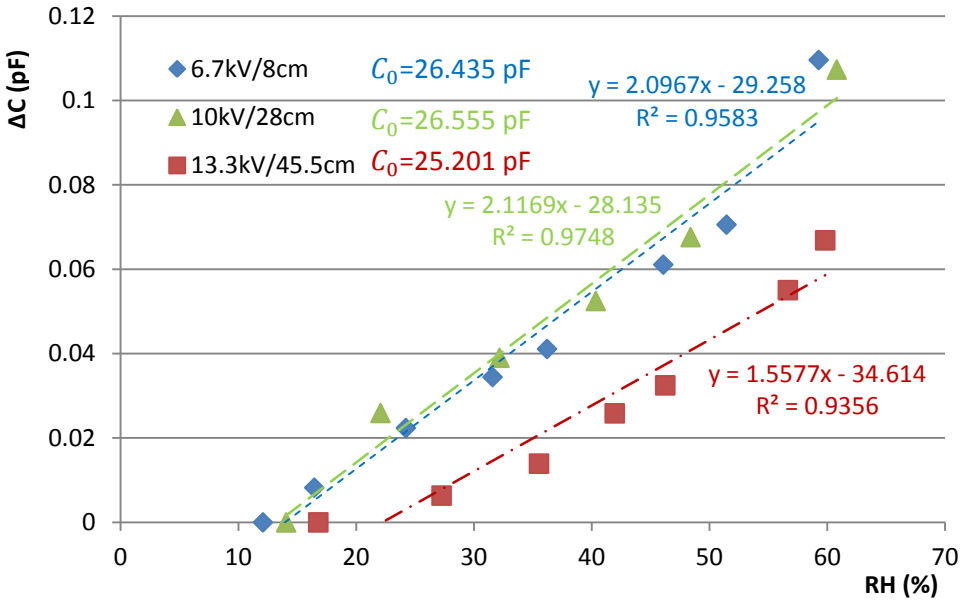

Figure 6.7: Effect of electric field indicated by the experimental results of sensors E2, E7, and E8 from 12% to 60% RH (detected by oscillator circuit).

E2, **E7** and **E8** have the same electrospraying time and different electric field. The electrospraying voltage of **E2** is fixed at 10 kV, and **E7** is 3.3 kV less than **E2**, while **E8** is 3.3 kV more than **E2**. The distance is fixed when the Taylor cone formed under the applied voltage. When the distance is too long, there will be some small droplets deposited on top of the IDE which will affect the sensitivity of the sensor. As shown in Figure 6.7, **E8** has the lowest sensitivity with longest distance. The electric fields are 6.7 kV/8 cm=0.84 kV/cm, 10 kV/28 cm=0.36 kV/cm, and 13.3kV/45.5 cm=0.29 kV/cm, respectively. The lower sensitivity of **E8** shows that lower electric field with longer distance results in poorer sensitivity. Sensors **E2** and **E7** have similar linearity and sensitivity (capacitance change), even though electrospraying voltage, distance, and

electric field were not the same. More research is required to be able to draw conclusions about the effect of electric field on sensor performance.

The effect of electrospraying voltage is illustrated in Figure 6.8 for two similar devices fabricated with different voltages. Sensor **E4** was fabricated using a 15kV/30cm field, corresponding to the lowest voltage when Taylor cone forms. On the other hand, sensor **E9** was fabricated with a 25kV/30cm field; i.e., the highest voltage above which the Taylor cone disappears. It was found that **E4** has more nanoparticles and nanofibers between nanoparticles than **E9**. Lower voltage results in a higher density of nanoparticles, which will increase the sensitivity of the sensor.

6.2.3. Effect of Deposition Methods

Different deposition methods will result different sensor performances. The comparison between electrospraying PI (**E6**), spin-on uniform PI (**S1**), and bare sample (**B1**) are shown in Figure 6.9.

In order to have accurate results, an LCR meter is used during these three experiments. Bare sample means nothing covers the top of the IDEs. As the RH increases, the water vapor forms a thin water film over the IDEs and the capacitance will increase. As shown in Figure 6.9, the sensor without a PI film exhibits the highest capacitance change but the worst linearity. This highly nonlinear behaviour could be due to the increase in conduction current as the thickness of the water film increases. This also explains why 5 minutes electrospraying time has the highest capacitance change in Figure 6.5. Figure 6.9 also shows that electrospraying PI and spin-on uniform PI have the close sensitivity and linearity. From 10% to 40% RH spin-on uniform PI has a slightly higher sensitivity, and from 50% to 60% RH electrospraying PI shows more sensitivity. As electrospraying method is significantly simpler than spin-on method, electrospraying PI provides a more economical and flexible technique to deposit PI.

(a)

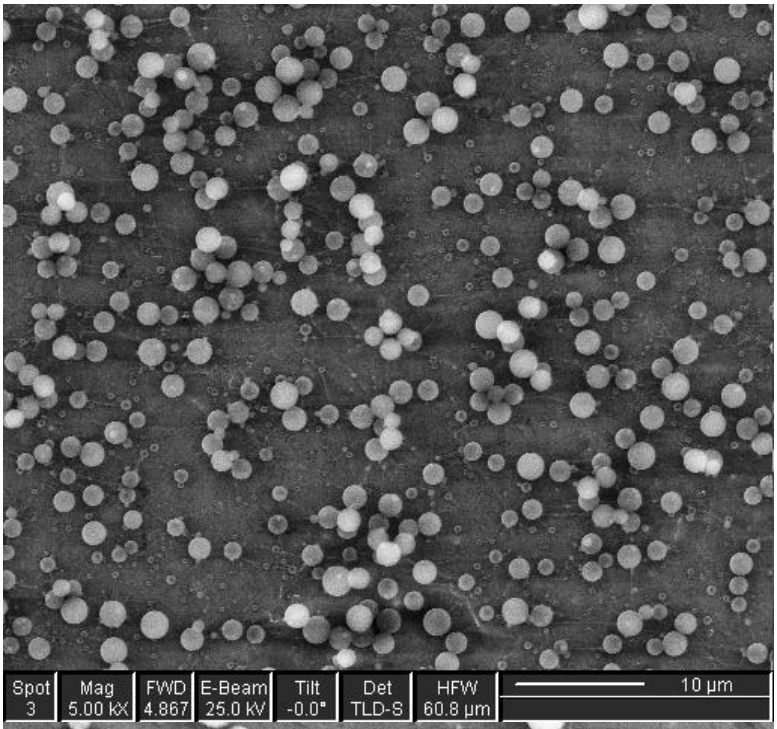

(b)

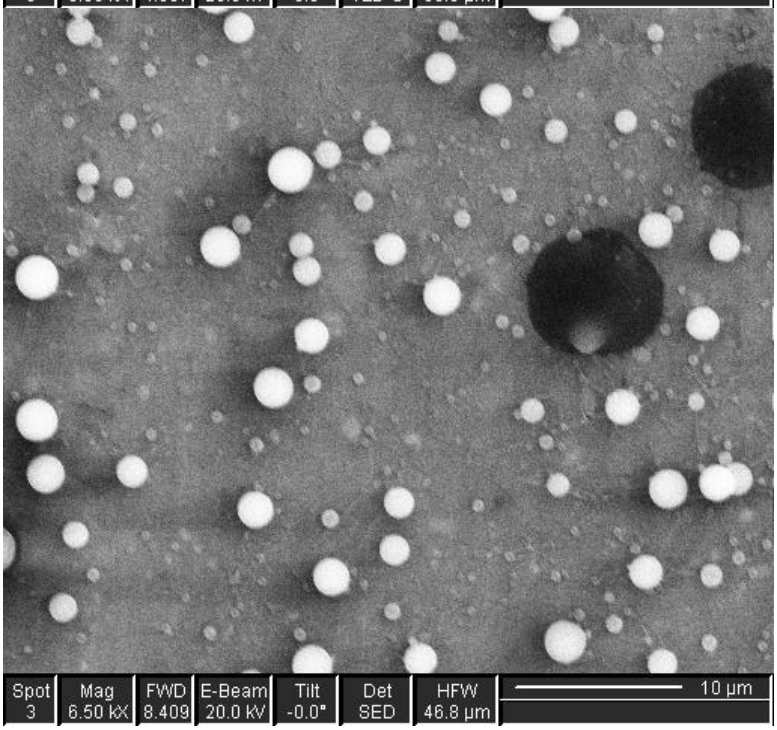

Figure 6.8: Effect of electrospraying voltage: SEM images of (a) E4 with 15/30 kV/cm and (b) E9 with 25/30 kV/cm electrosprayed for 30 min.

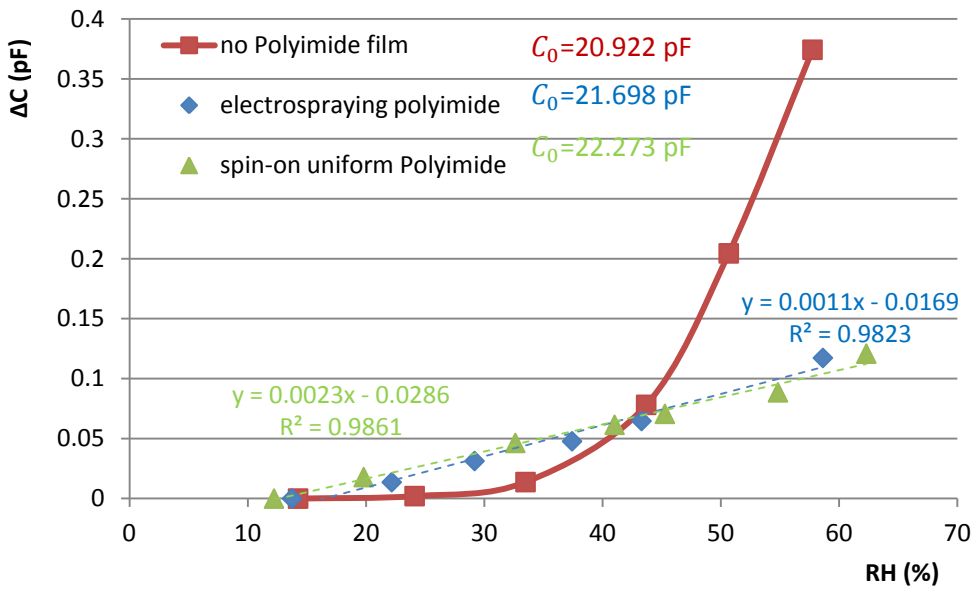

Figure 6.9: Effect of film thickness on linearity and sensitivity under 65% RH (detected by LCR meter).

6.3. Specifications of the Capacitive RH Sensor

There are many important specifications should be kept in mind when choosing a humidity sensor including: accuracy, repeatability, interchangeability, long-term stability, ability to recover from condensation, resistance to chemical and physical contaminants, size, packaging, and cost effectiveness [5].

The capacitive RH sensor mentioned in this paper has a small size which is 5 mm×5 mm. The fabrication costs can be decreased because of the simple structure and simple fabrication steps.

Some other specifications of the capacitive RH sensor are discussed in this section. The RH sensor **E6** is used in the following sections.

6.3.1. *Repeatability between increasing and decreasing RH*

Figure 6.10 compares the capacitance change difference between increasing RH and decreasing RH with the same electrospraying PI sensor **E6** from 15% to 97% RH. The average time between taking data points was 23 minutes. As shown in Figure 6.10, from 15% to 40% RH, the capacitance change between increasing RH and decreasing RH are repeatable; from 40% to 70% RH, the capacitance change are similar; from 70% to 97% RH, the capacitance change depend on the prior state of the sensor.

This sensor has a good repeatability between increasing RH and decreasing RH from 15% to 70% RH.

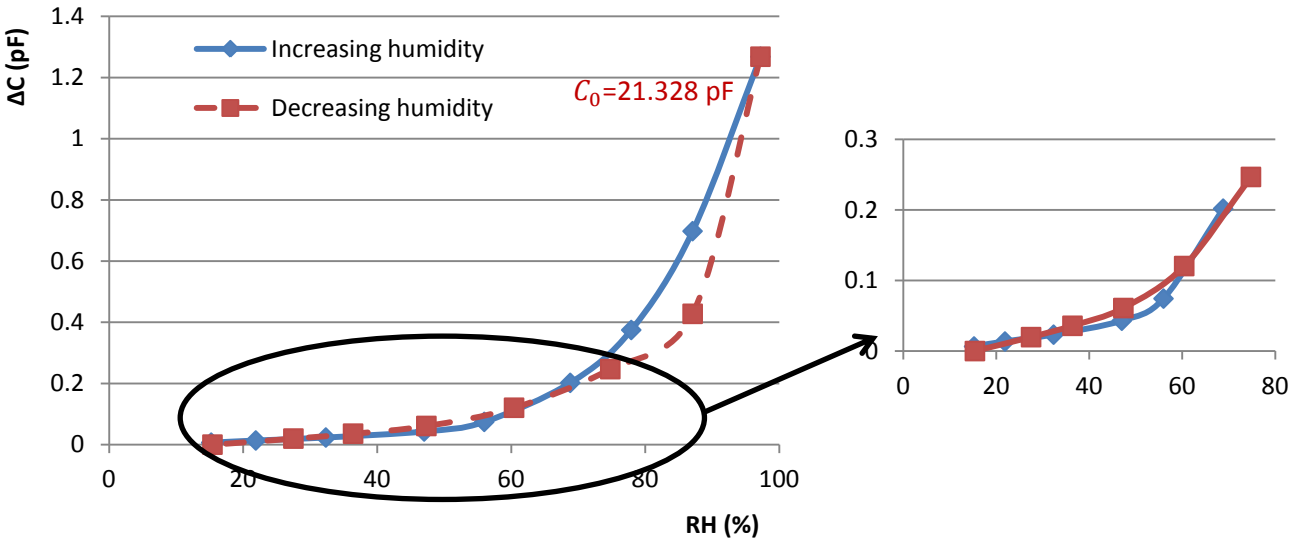

Figure 6.10: Capacitance change comparision between increasing RH and decreasing RH of sensor E6 (detected by LCR meter).

6.3.2. *Stability*

The stability of the RH sensor is tested by comparing the capacitance change with RH (see Figure 6.11). Figure 6.11 (a) shows the capacitance change of the RH sensor **E6** detected by LCR meter, and figure 6.11 (b) shows the RH detected by humidity sensor HIH-4000-003. The test lasted for 6 hours.

Limited by the experiment set-up, the RH could not be kept stable for 6 hours and RH started to change after about 2 hours. The first 80 minutes are plotted in Figure 6.12.

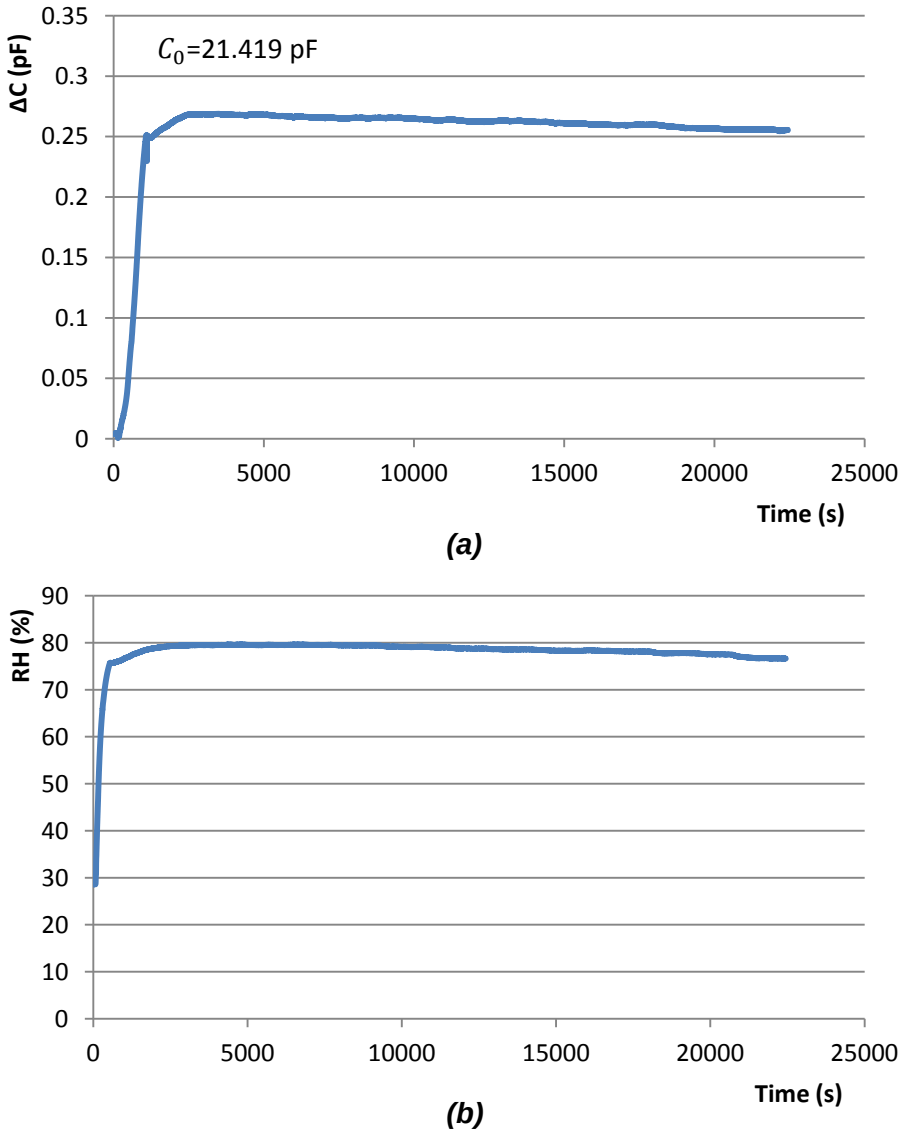

Figure 6.11: Test the RH sensor's stability with comparing the humidity change and the capacitance change: (a) the sensor E6's capacitance change (detected by LCR meter), (b) the humidity change measured by humidity sensor HIH-4000-003. (Data was taken at 2 second intervals)

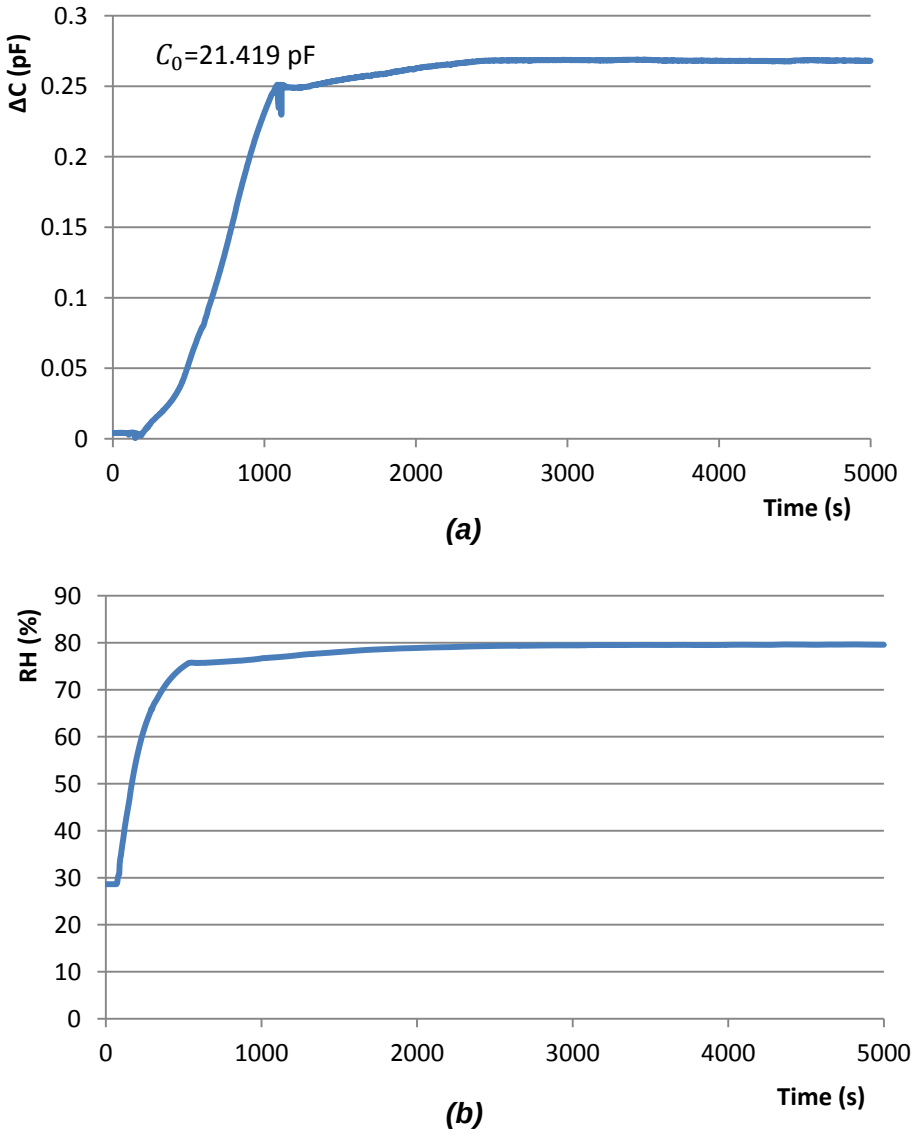

Figure 6.12: First 80 minutes of the 6 hours sensor E6 stability test. (Data was taken at 2 second intervals).

6.3.3. *Response Time*

The response time of the capacitance change of the RH sensors **E6** and HIH-4000-003 were measured at the same time.

As shown in Figure 6.13, from 12% to 21% RH, the response time of the RH sensor is around 5 minutes, which is similar to HIH-4000-003.

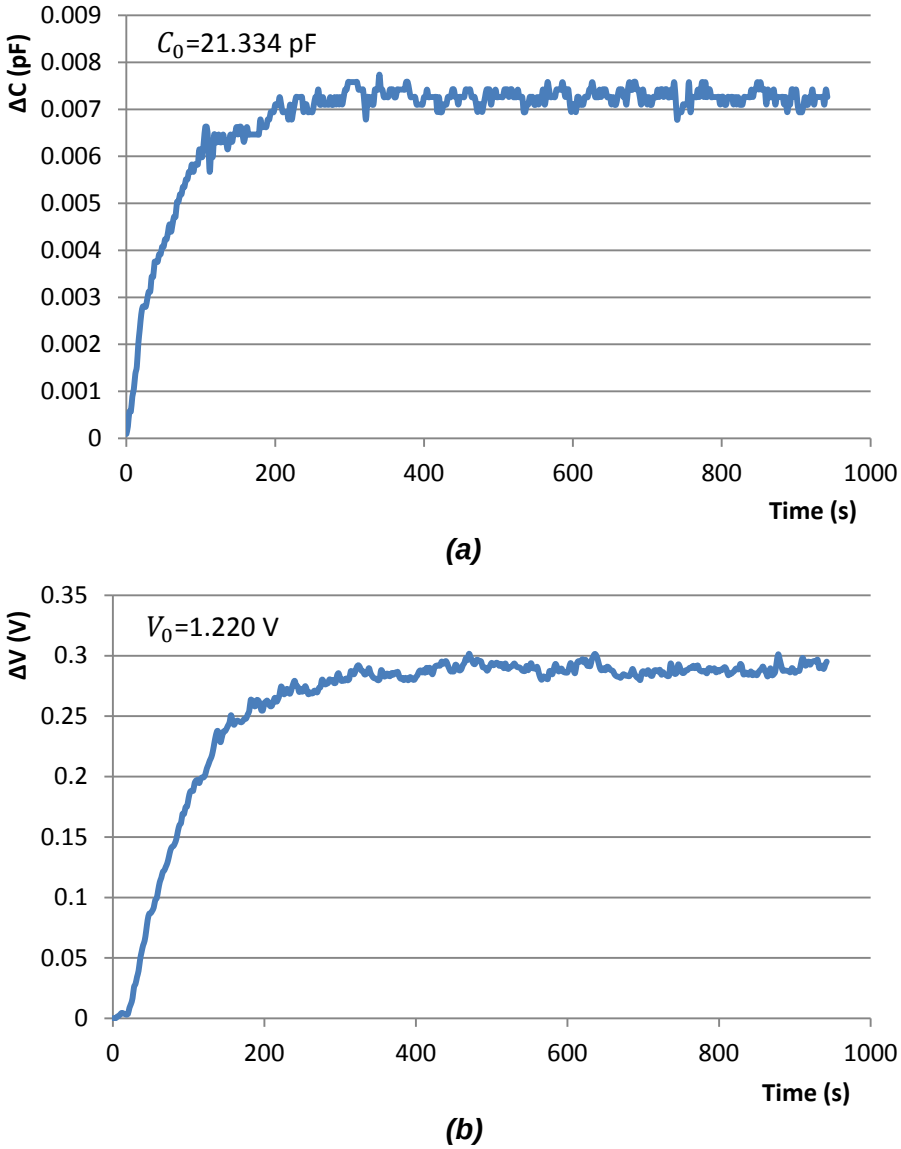

Figure 6.13: Response time of (a) capacitance change of the sensor E6 (detected by LCR meter) and (b) voltage change of the humdity sensor HIH-4000-003 from 12% to 21% RH. (Data is taken at 2 second intervals)

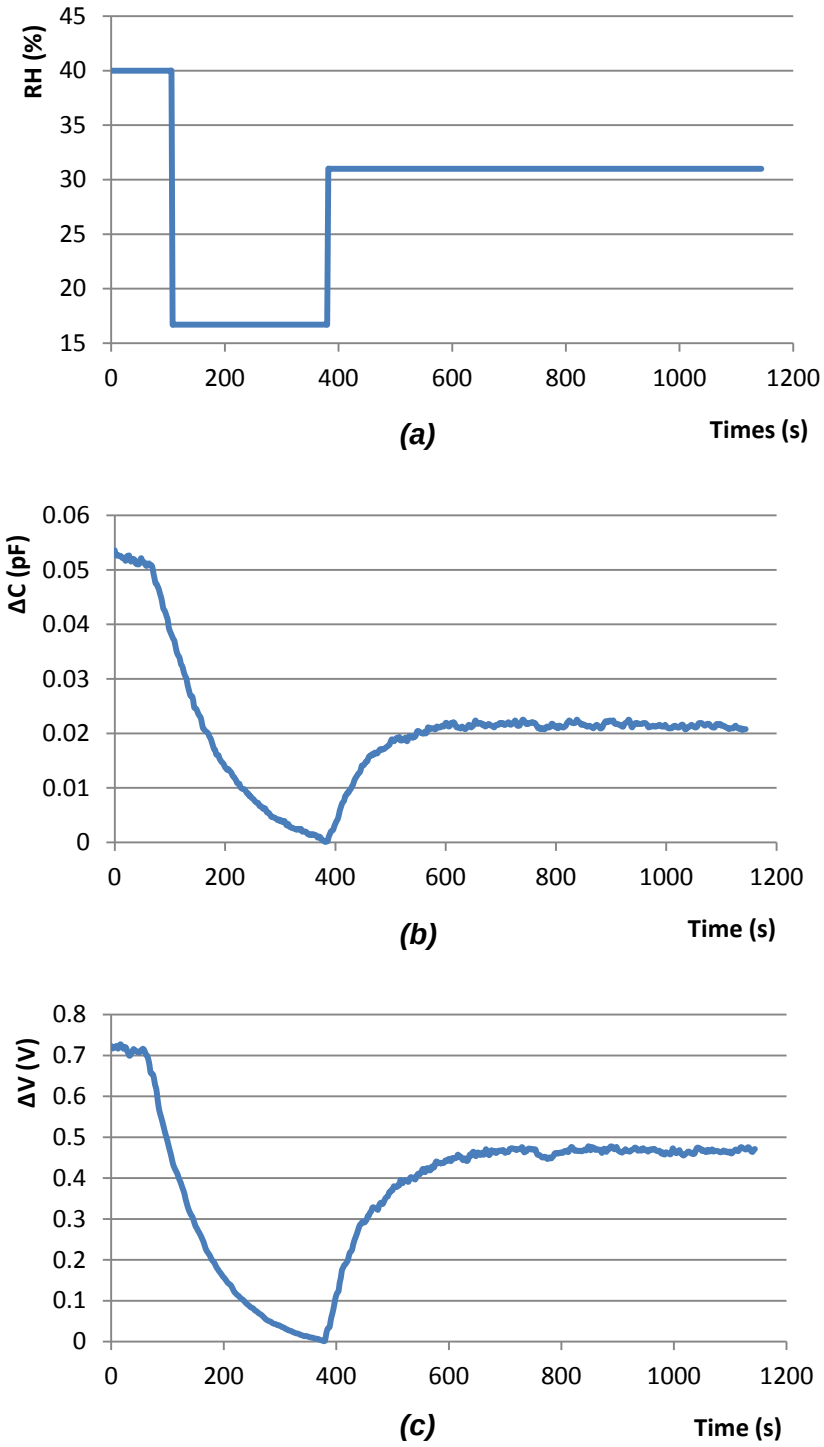

Figure 6.14: The similar changing tendency (a) from 39% to 17% RH, and then increase to 32% RH between (b) the capacitance of the sensor E6 (detected by LCR meter) and (c) the voltage detected by HIH-4000-003. (Data was taken at 2 second intervals)

The capacitance change of the capacitive RH sensor **E6** and the voltage change of the humidity sensor HIH-4000-003 are detected at the same time as shown in Figure 6.14. The result of RH capacitive sensor **E6** are in good agreement with the measured result from humidity sensor HIH-4000-003.

6.4. Measurements with the developed interface electronics

In practice, we use either the C-V or C-F circuits to measure the output of RH sensors.

6.4.1. Measurements with Capacitive Sensing Circuit

The experiment (see Figure 6.15) set-up with C-V circuit is nearly identical to the set-up used for the LCR meter. The LCR meter is replaced by a C-V circuit and the other multimeter.

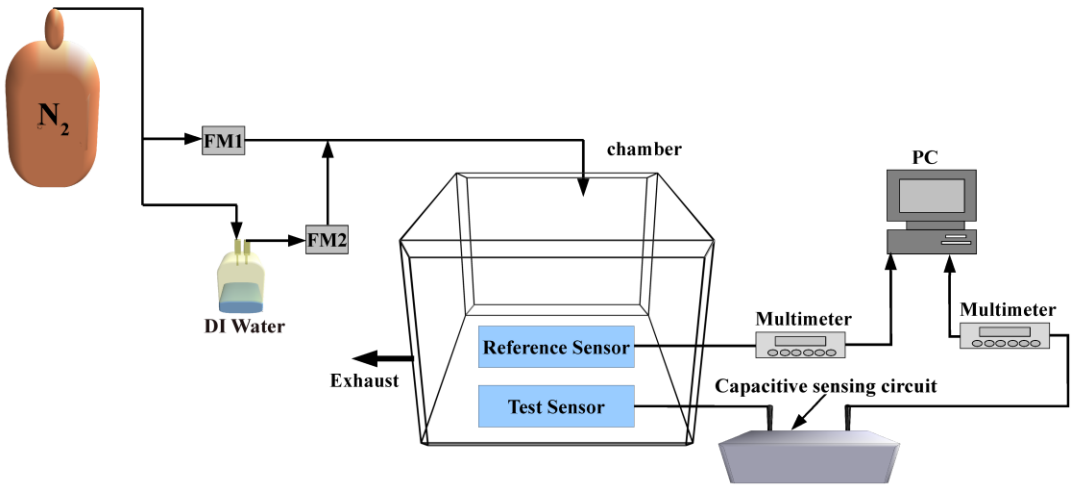

Figure 6.15: Measurement setup for C-V circuit.

The output voltage of the humidity sensor HIH-4000-003 read from the multimeter can be converted to RH from:

$$RH = (V - 0.85)/0.03 \quad (9)$$

where V is the voltage read by multimeter from HIH-4000-003 sensor.

Three experimental results with C-V circuit are shown in Figure 6.16. The “RH (%)” shown in the figure is calculated from equation (9); the “Voltage (V)” shown in the figure is the output voltage read from the test sensor.

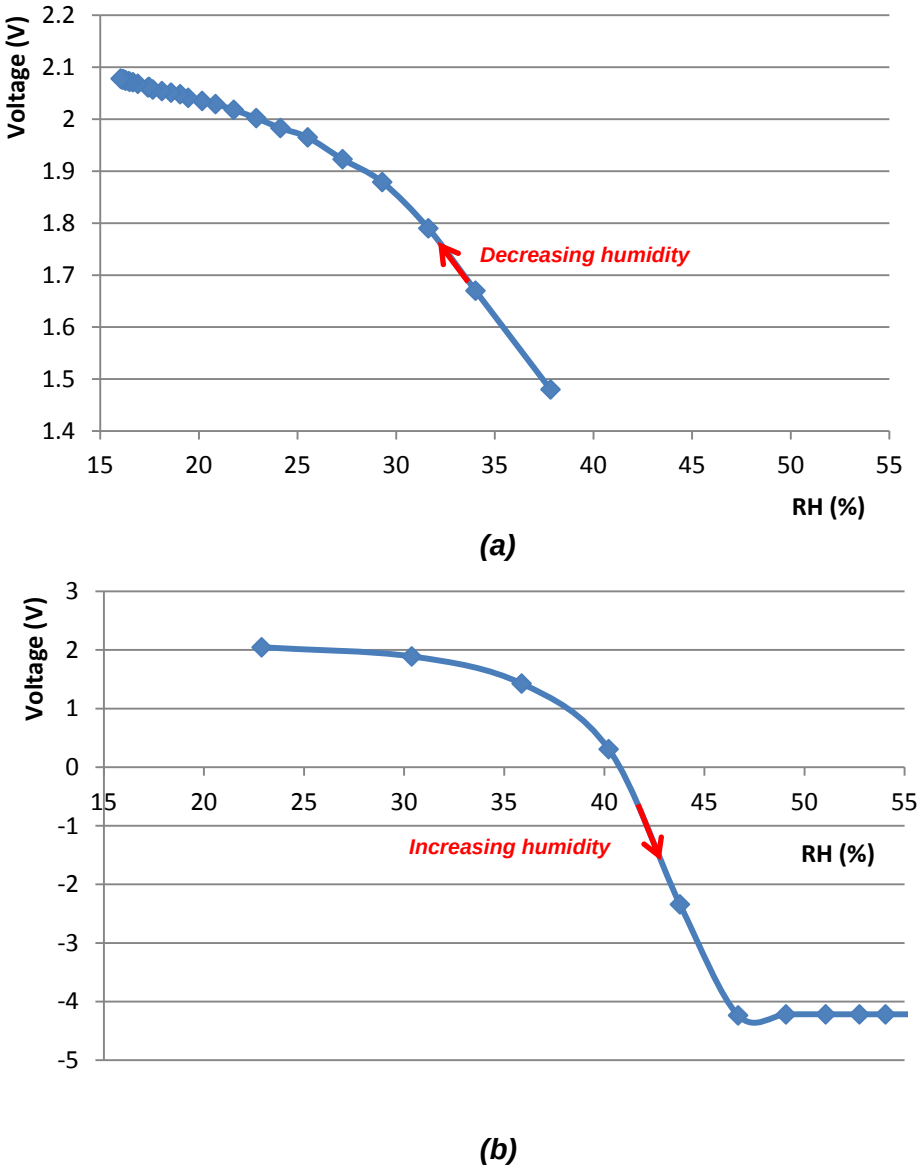

Figure 6.16: Experimental results of E10 when the RH sensor is connected between Electrode- and Electrodemid connectors: (a) RH is decreasing; (b) RH is increasing

Humidity in Figure 6.16 (a) and (b) is detected when the RH sensor E10 is connected to *Electrode-* and *Electrodemid* connectors, and a 22 pF capacitor is

connected to *Electrode+* and *Electrodemid* connectors as a reference capacitor. Results shown in Figure 6.16 (a) and (b) are obtained when RH was decreasing in the first case, and increasing in the second. It is shown in Figure 6.16 (b) that from 45% to 55% RH, the output voltage of the test sensor stays at -4.2 V; i.e., the saturation level of the electronics. As the RH increases, the output voltage keeps on decreasing.

Figure 6.17 shows the result when the RH sensor E11 is connected between *Electrode+* and *Electrodemid* connectors, and a 22 pF capacitor is connected between *Electrode-* and *Electrodemid* connectors as a reference capacitor. The output voltage is increasing when the RH is increasing.

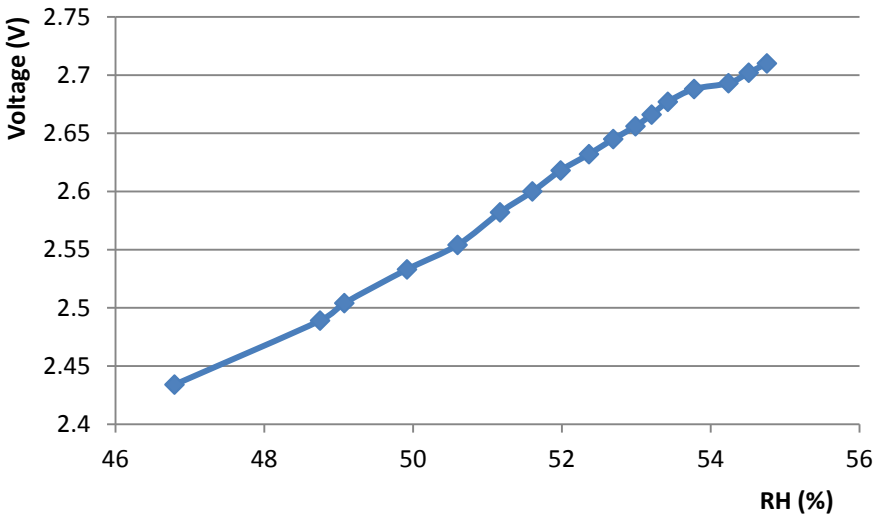

Figure 6.17: Experimental result of E11 when the RH sensor is connected between Electrode+ and Electrodemid connectors.

6.4.2. Measurements with Oscillator Circuit

The experiment set-up is shown in Figure 6.18 which is nearly identical to the setup in Figure 6.1. A frequency counter (Agilent 53132A 225MHz Universal Counter) was used to measure the signal frequency from the C-F circuit.

The frequency read from frequency counter can be converted to capacitance from equation (8). The experimental results of RH sensor E12 with C-F circuit are shown

in Figure 6.19. The “RH (%)” shown in the figure is calculated from equation (9); the “ΔC (pF)” shown in the figure is the difference of the capacitance calculated from equation (8).

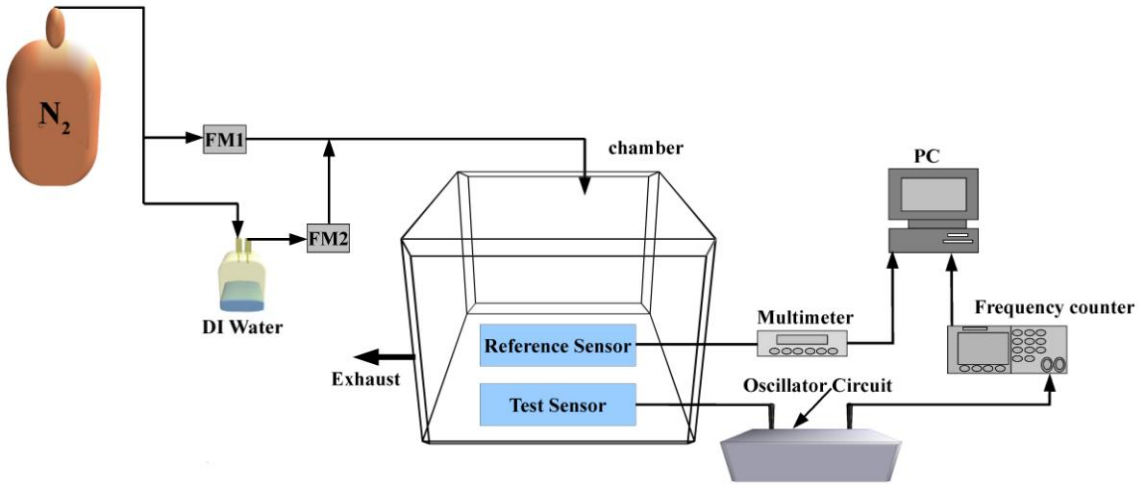

Figure 6.18: Measurement setup for C-F circuit.

Results in Figure 6.19, (a) and (b) are detected from the same RH sensor **E12**. Figure 6.19 (a) shows the results when tap water was used in the reservoir while Figure 6.19 (b) is for results with DI water (both tap water and DI water are used in creating the water vapor). As shown in figure (a), the capacitance of the IDE with tap water is increasing quickly and non-linear; and the capacitance of the IDE with DI water shows a better linearity in figure (b).

The difference in results between tap water and DI water is assumed to be due to the existence of the mineral ions. It is postulated that droplets of water will form in pipes and containers, especially as the RH level goes above 40%. Some of these droplets will travel with the nitrogen flow and can end up on the surface of the sensors. Minerals in tap water will increase the conduction current that over the IDE structure. Conduction current increases faster than capacitance current due to the mineral ions, which causes the perceived fast increase in capacitance when testing with tap water.

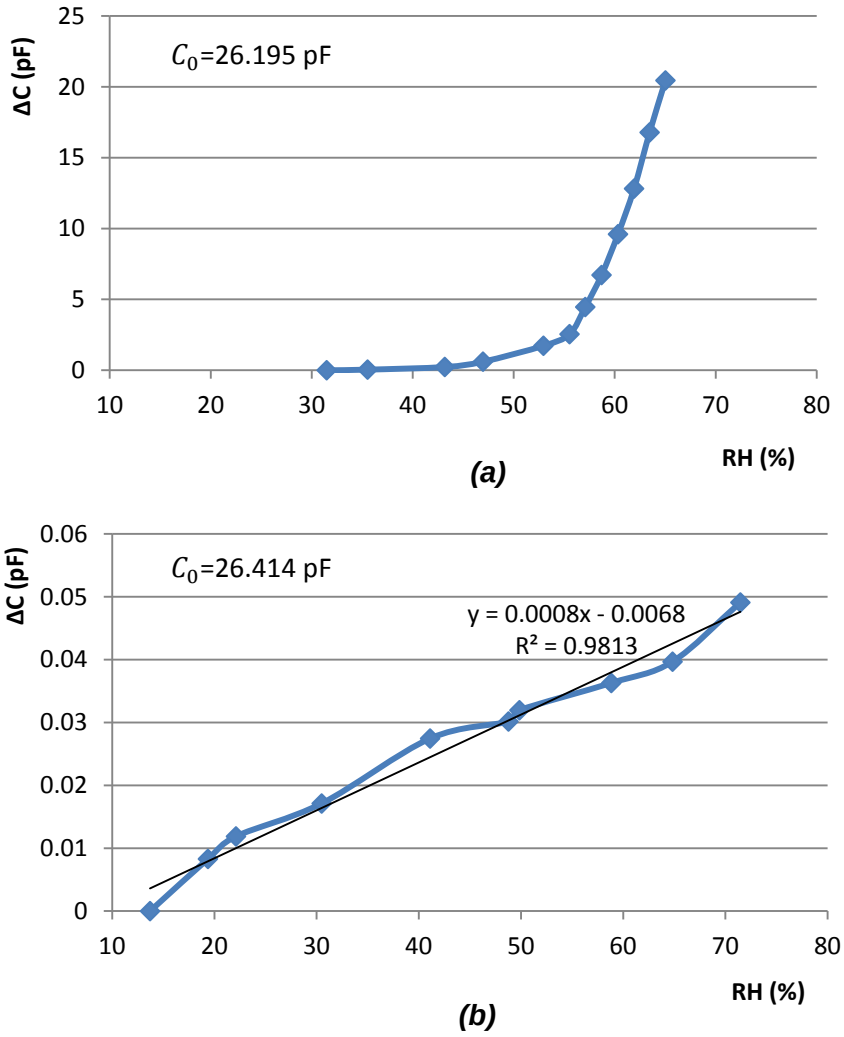

Figure 6.19: Experimental results of E12: (a) with tap water from 31% to 65% RH, (b) with DI water from 13% to 71% RH.

Another experimental result of RH sensor **E13** with decreasing RH is shown in Figure 6.20.

Comparing to the experiment with C-V circuit, the method with C-F circuit has the advantage that it can cove a wider range of capacitance. As the capacitance can be detected over a wider dynamic range, the RH can be detected from 0% to 100%.

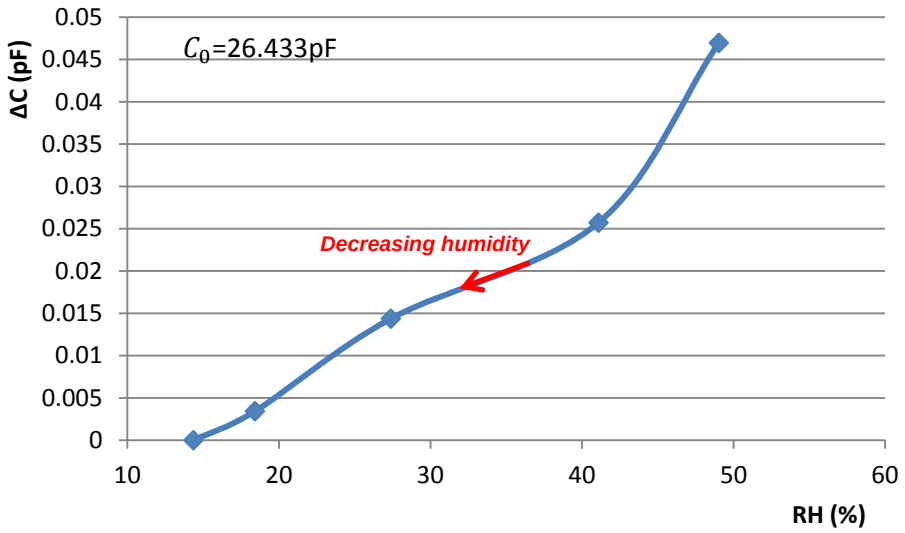

Figure 6.20: Experimental result of E13 with DI water which is used in creating the water vapor.

7. Conclusions and future work

Fabrication of a capacitive RH sensor based on polyimide nanoparticles was discussed in this thesis. Capacitive RH sensors were widely used because of their linearity in a wide range of relative humidity. Operation of capacitive RH sensors is based on the change of the dielectric constant of a sensitive material as a function of the RH in the surrounding environment [25]. PI was used as the sensing material in the thesis due to its low hysteresis, linear behavior, and stability over a wide temperature range. PI exhibited good sensitivity to relative humidity changes [4]. PI also shows good stability when exposed to most chemicals, which has led to its widespread application in electronics industry as a protective layer. However, this stability also made the process of patterning PI complicated. A simplified fabrication process, electrospraying, was proposed to overcome these shortcomings.

The capacitive RH sensors were realized through depositing the PI nanoparticles on top of interdigitated metallic electrodes on a glass substrate. The interdigitated structure was used for the following advantages: simple structure, more contact area, and relatively planar surface. The electrospraying method could be carried outside a cleanroom in contrast to the traditional spin-on method. The electrospraying process was also flexible and could be used to build RH sensors on printed circuit board (PCB), thus reducing manufacturing costs of such sensor systems. Many electrospraying parameters were studied to improve the performance of the RH sensors. The performance of the sensors made through electrospraying process and spin-on process was also compared. The result can be gotten that the higher film density result in higher linearity and sensitivity, and the RH sensor with PI has higher linearity than the one without PI. The RH sensors with electrosprayed PI exhibited a similar level of sensitivity and linearity compared to the RH sensor with spin-on uniform PI. Experimental results also showed that the humidity sensors proposed in this thesis provide stable data in a short time with low hysteresis when increasing and decreasing humidity.

Two interface electronics, capacitance sensing circuit and oscillator circuit, were developed to test the output of the RH sensor. Capacitance sensing circuit is more sensitive while the oscillator is more flexible and can cover a wider range of capacitance.

7.1. Contributions

The work presented in this thesis has so far led to the following publications:

1. F. Aezinia, **Y. Wang**, and B. Bahreyni, "Touchless capacitive sensor for hand gesture detection," *Proceeding Sensors, 2011 IEEE*, pp.546-549, Oct. 2011.

2. F. Aezinia, **Y. Wang**, and B. Bahreyni, "Three dimensional touchless tracking of objects using integrated capacitive sensors," IEEE Transactions on Consumer Electronics, vol.58, no.3, pp.886-890, August 2012.

3. **Y. Wang**, M.S. Hajhashemi, and B. Bahreyni, “A Capacitive Relative Humidity Sensor using Polymer Nanoparticles,” *Proceeding of the IEEE Sensors Conference*, pp.418-421, Oct. 2012.

7.2. Future work

Based on the achievements in the thesis, recommend future work include:

1. The RH sensor works well under 60% RH, but the linearity is poor after 60% RH. More research has to be conducted to solve this problem.

2. The RH sensor shows good linearity under 60% RH, but the capacitance change is too small. We need find a way to increase sensitivity for easier detection.

3. The RH sensor provides good results with PI nanoparticles. Next step is fabricating RH sensor with PI nanofibers, which may increase the performance of the RH sensor and its stability.

Bibliography

[1] R. Fenner and E. Zdankiewicz, "Micromachined water vapor sensors: a review of sensing technologies," *IEEE Sensors Journal,* vol. 1, no. 4, pp. 309-317, 2001.

[2] A. S. mohammed and A. Mahmud, "Development of electronic hygrometer system," *AU Journal Tech,* pp. 48-57, 2007.

[3] A. Hartzell and M. da Silva, "Reliability issues in miniaturized sensors: importance of standards. what is needed?," *IEEE Sensors,* vol., no., pp.44, 28-31 Oct. 2007

[4] J.-H. Kim, S.-M. Hong, J.-S. Lee, B.-M. Moon and K. Kim, "High sensitivity capacitive humidity sensor with a novel polyimide design fabricated by MEMS technology," *4th IEEE International Conference on Nano/Micro Engineered and Molecular Systems,* pp.703-706, 5-8 Jan. 2009.

[5] D. K. Roveti, "Choosing a humidity sensor: a review of three technologies," 2001 < http://www.sensorsmag.com/sensors/humidity-moisture/choosing-a-humidity-sensor-a-review-three-technologies-840>.

[6] J. Green and I. Dyer, "Measurement of humidity," *Anaesthesia and Intensive Care Medicine,* vol. 10, no. 1, pp. 45-47, 2009.

[7] Z. Chen and C. Lu, "Humidity Sensors: A review of materials and mechanisms," *Sensor Letters,* vol. 3, no. 4, pp. 274-295, 2005.

[8] Z. Rittersma, "Recent achievements in miniaturised humidity sensors - a review of transduction techniques," *Sensors and Actuators A: Physical,* vol. 96, no. 2-3, pp. 196-210, 2002.

[9] V. Mohan, "EI 602 Process Control Instrumentation - I", Lecture notes, College of Engineering Kidangoor, Kidangoor, Kerala, August 28, 2010.

[10] Yankee Environmental Systems, Inc. "chilled mirror hygrometers," 2005 < http://www.yesinc.com/products/data/cmh/humidityds.pdf>.

[11] L. Gu, Q.-A. Huang and M. Qin, "A novel capacitive-type humidity sensor using CMOS fabrication technology," *Sensors and Actuators B: Chemical,* vol. 99, no. 2-3, pp. 491-498, 2004.

[12] X. Lv, Y. Li, L. Hong, D. Luo and M. Yang, "A highly water-resistive humidity sensor based on silicon-containing polyelectrolytes prepared by one-pot method," *Sensors and Actuators B: Chemical,* vol. 124, no. 2, pp. 347-351, 2007.

[13] N. M. Kiasari, S. Soltanian, B. Gholamkhass and P. Servati, "Room temperature ultra-sensitive resistive humidity sensor based on single zinc oxide nanowire," *Sensors and Actuators A: Physical,* vol. 182, pp. 101-105, 2012.

[14] K.-P. Yoo, L.-T. Lim, N.-K. Min, M. J. Lee, C. J. Lee and C.-W. Park, "Novel resistive-type humidity sensor based on multiwall carbon nanotube/polyimide

[15] "IOM 87 Module B2 2 pps" (2010) <http://ebookbrowse.com/iom-87-module-b2-2-pps-d24579095> (Accessed: 29 Jan 2013).

[16] B. Okcan and T. Akin, "A thermal conductivity based humidity sensor in a standard CMOS process," *17th IEEE International Conference on Micro Electro Mechanical Systems (MEMS)*, vol., no., pp. 552- 555, 2004.

[17] J. Corres, I. Matias, M. Hernaez, J. Bravo and F. Arregui, "Optical fiber humidity sensors using nanostructured coatings of SiO_2 nanoparticles," *IEEE Sensors Journal,* vol. 8, no. 3, pp. 281-285, March 2008.

[18] J. Mathew, Y. Semenova and G. Farrell, "A miniature optical humidity sensor," *IEEE Sensors,* vol., no., pp.2030-2033, 28-31 Oct. 2011

[19] B. Wang, F. Zhang, F. Pang and T. Wang, "An optical fiber humidity sensor based on optical absorption," *ACP. Asia Communications and Photonics Conference and Exhibition,* vol., no., pp.1-6, 13-16 Nov. 2011

[20] A. Urrutia, P. Rivero, J. Goicoechea, F. Arregui and I. Matias, "Optical sensor based on polymer electrospun nanofibers for sensing humidity," *Fifth International Conference on Sensing Technology (ICST), v*ol., no., pp.380-383, Nov. 28 2011-Dec. 1 2011

[21] F. Pascal-Delannoy, B. Sorli and A. Boyer, "Quartz crystal microbalance (QCM) used as humidity sensor," *Sensors and Actuators A: Physical,* vol. 84, no. 3, pp. 285-291, 2000.

[22] L. Sheng, C. Yuquan and L. Yang, "A novel SAW humidity sensor based on electrosprayed polymerized electrolyte film," *Third International Conference on Measuring Technology and Mechatronics Automation (ICMTMA),* vol.1, no., pp.214-217, 6-7 Jan. 2011.

[23] V. Ferrari, D. Marioli, A. Taroni, E. Ranucci and P. Ferruti, "Development and application of mass sensors based on flexural resonances in alumina beams," *IEEE Transactions on Ultrasonics, Ferroelectrics and Frequency Control,* vol. 43, no. 4, pp. 601-608, July 1996.

[24] Y. L. Yang, L. H. Lo, I. Y. Huang, H. Chen, W. S. Huang and S. Huang, "Improvement of polyimide capacitive humidity sensor by reactive ion etching and novel electrode design," *Proceedings of IEEE* in *Sensors,* 2002.

[25] L. Juhasz, A. Vass-Vamai, V. Timar-Horvath, M. Desmulliez and R. Dhariwal, "Porous alumina based capacitive MEMS RH sensor," *Symposium on Design, Test, Integration and Packaging of MEMS/MOEMS,* pp.381-385, *2008.*

[26] L. J. Golonka, B. W. Licznerski, K. Nitsch and H. Teterycz, "Thick-film humidity sensors," *Measurement Science and Technology,* vol. 8, no. 1, p. 92, 1997.

[27] J. Fraden, Handbook of modern sensors: physics, designs, and applications (handbook of modern sensors), SpringerVerlag, 2003.

[28] J. Steele, G. Fitzpatrick and M. Brett, "Capacitive humidity sensors with high sensitivity and subsecond response times," *IEEE Sensors Journal,* vol. 7, no. 6, pp. 955-956, June 2007.

[29] Z. Rittersma, A. Splinter, A. Bodecker and W. Benecke, "A novel surface-micromachined capacitive porous silicon humidity sensor," *Sensors and Actuators B: Chemical,* vol. 68, no. 1-3, pp. 210-217, 2000.

[30] W. Qu and J.-U. Meyer, "A novel thick-film ceramic humidity sensor," *Sensors and Actuators B: Chemical,* vol. 40, no. 2-3, pp. 175-182, 1997.

[31] A. Tetelin and C. Pellet, "Modeling and optimization of a fast response capacitive humidity sensor," *IEEE Sensors Journal,* vol. 6, no. 3, pp. 714-720, June 2006.

[32] A. Tetelin, C. Pellet, A. Achen and M. Toepper, "Capacitive humidity sensors based on oxidized PhotoBCB polymer films: enhanced sensitivity and response time," *IEEE Sensors,* vol., no., pp.4 pp., Nov. 2005

[33] H. Lee, S. Jung, H. Kim and J. Lee, "High-performance humidity sensor with polyimide nano-grass," *International Solid-State Sensors, Actuators and Microsystems Conference, TRANSDUCERS 2009,* vol., no., pp.1011-1014, June 2009

[34] A. L. Andrady, Science and technology of polymer nanofibers, John Wiley & Sons, Inc., 2008.

[35] V. S. Rao, "Collection of higihly aligned electrostrictive graft elastomer nanofibers using electrospinning in a vacuum environment," MSc dissertation, Kansas State Univeristy, 2009.

[36] T. Subbiah, G. S. Bhat, R. W. Tock, S. Parameswaran and S. S. Ramkumar, "Electrospinning of nanofibers," *Journal of Applied Polymer Science,* vol. 96, no. 2, pp. 557-569, 2005.

[37] J. Doshi and D. Reneker, "Electrospinning process and applications of electrospun fibers," *Conference Record of the 1993 IEEE Industry Applications Society Annual Meeting,* vol., no., pp.1698-1703 vol.3, 2-8 Oct 1993.

[38] G. Taylor, "Disintegration of water drops in an electric field," *Proc. R. Soc. Lond. A,* vol. 280, pp. 383-397, 1964.

[39] M. M. Hohman, M. Shin, G. Rutledge and M. P. Brenner, "Electrospinning and electrically forced jets. I. Stability theory," *Physics of Fluids,* vol. 13, no. 8, pp. 2201-2220, 2001.

[40] L. G. D. Mendonca and R. C. Ibrahim, "Interdigitated-type microsensor to measure solution concentration," *ABCM Symposium Serise in Mechatronics, vol.2, pp. 465-468*, 2006.

[41] J. S. Kim, K.-Y. Kwak, K.-H. Kwon, N.-K. Min and M.-S. Kang, "A locally cured polyimide-based humidity sensor with high sensitivity and high speed," *IEEE Sensors,* vol., no., pp.434-437, 26-29 Oct. 2008.

[42] D. D. Chung, Materials for electronic packaging, Butterworth Heinemann, 1995.

[43] F. Aezinia, Y. Wang and B. Bahreyni, "Three dimensional touchless tracking of objects using integrated capacitive sensors," *IEEE Transactions onConsumer Electronics,* vol. 58, no. 3, pp. 886-890, August 2012.

[44] B. George, H. Zangl, T. Bretterklieber and G. Brasseur, "A combined inductive capacitive proximity sensor for seat occupancy detection," *IEEE Transactions on Instrumentation and Measurement,* vol. 59, no. 5, pp. 1463-1470, May 2010.